# Holocene phototrophic community and anoxia dynamics in meromictic Lake Jaczno (NE Poland) using high-resolution hyperspectral imaging and HPLC data.

Stamatina Makri[1], Andrea Lami[2], Luyao Tu[1], Wojciech Tylmann[3], Hendrik Vogel[4,] Martin Grosjean[1]

[1]Institute of Geography & Oeschger Centre for Climate Change Research, University of Bern, Hallerstrasse 12, 3012 Bern, Switzerland

[2]ISE-CNR Institute of Ecosystem Study, 50 Largo Tonolli, 28922 Verbania Pallanza, Italy

[3]Faculty of Oceanography and Geography, University of Gdansk, Bazynskiego 4, PL-80952 Gdansk, Poland

[4]Institute of Geological Sciences & Oeschger Centre for Climate Change Research, University of Bern, 3012, Bern, Switzerland

*Correspondence to*: Stamatina Makri (stamatina.makri@giub.unibe.ch)

**Abstract.** Global spread of hypoxia and ~~altered mixing regimes~~less frequent mixing in ~~freshwater systems~~lakes is a growing major environmental concern. Climate change and human impact are expected to increasingly deteriorate aquatic ecosystems. The study of processes and drivers of such changes in the past provides a great asset for prevention and remediation in the future. We used a multi-proxy approach combining high-resolution bulk pigment data measured by Hyperspectral Imaging (HSI) ~~pigment data~~, with lower resolution specific ~~HPLC~~ chlorophylls and carotenoids measured by HPLC to examine Holocene trophic state changes and anoxia evolution in meromictic Lake Jaczno, NE Poland. A redundancy analysis RDA including pollen-inferred vegetation cover, temperature and human impacts provides insight into specific conditions and drivers of changing trophic and redox states in the lake. Anoxic and sulfidic conditions established in Lake Jaczno after initial basin infilling 9500 years ago. Until 6700 cal BP, lake trophy was relatively low, water turbidity was high, and green sulfur bacteria (GSB) were abundant within the phototrophic community, suggesting a deep oxic–anoxic boundary and weak stratification. The period between 6700–500 cal BP is characterized by constantly increasing lake production and a gradual shift from GSB to purple sulfur bacteria (PSB), suggesting a shallower oxic–anoxic boundary and pronounced stratification. Yet, the presence of spheroidene and speroidenone in the sediments indicates intermittent anoxia. After 500 cal BP, increasing human impact, deforestation and intensive agriculture promoted lake eutrophication, with a shift to PSB dominance and establishment of permanent anoxia and meromixis. Our study unambiguously documents the legacy of human impact on processes determining eutrophication and anoxia.

**Keywords:** Paleolimnology, Anoxia, Meromixis, Varved sediments, North–East Europe, Holocene, Sedimentary pigments, Human impact

## 1. Introduction

Eutrophication and subsequent oxygen depletion have become primary water quality issues for most freshwater and coastal marine ecosystems globally (Schindler, 2006; Jenny et al., 2016a). Rising mean global temperature

can potentially worsen lake anoxia by enhancing water stratification and algal blooms (Adrian et al., 2009; Woolway and Merchant, 2019). Higher lake trophy and reducing conditions in anoxic bottom waters can have diverse and profound negative effects on lake ecosystems, such as toxic algal blooms, fish kills, biodiversity loss (Smol, 2010; Battarbee and Bennion, 2012; Makri et al., 2019), and nutrient recycling into the water column from the sediment through redox processes (Gächter, 1987; Tu et al., 2019). Hence, the global spread of hypoxia grows into a major environmental concern (Diaz and Rosenberg, 2008).

Temporal and spatial extents of hypoxia/anoxia are influenced by both biological (aquatic production, organic matter decomposition) and physical (water stratification and lake mixing) factors (Smith and Schindler, 2009; Friedrich et al., 2014; Jenny et al., 2016b). Environmental and climatic effects such as temperature, seasonality and extreme events, catchment vegetation, land use, human impact and nutrient input affect lake production and oxygen supply in the bottom waters.

Observational data of anoxia and aquatic production cover usually only very short periods, which restricts the understanding of relevant processes and the knowledge of pre-disturbance conditions. This is most relevant for lake management or restoration. Although recent anoxia and eutrophication have been very well studied and understood (Naeher et al., 2013; Friedrich et al., 2014; Jenny et al., 2016a), less is known about the onset, cessation and specific conditions of these changes in the past due to the lack of effective and easily measurable proxies (Friedrich et al., 2014; Makri et al., 2020). More specifically, to assess lake trophy and/or bottom water oxygenation, proxies such as sedimentary pigments (Lami et al., 2000; Leavitt and Hodgson, 2001; Guilizzoni and Lami, 2002), lipid biomarkers (Naeher et al., 2012), diatom (Bennion and Simpson, 2011) and chironomid records (Little et al., 2000), stable isotopes (Pearson and Coplen, 1978), and redox sensitive elements such as Fe, Mn, Mo, V, and U (Naeher et al., 2013; Wirth et al., 2013; Costa et al., 2015), have been extensively used so far. Nonetheless, on long-term Holocene time-scales, most of these proxy records are typically established at a centennial resolution at best.

Laminated lake sediments are valuable archives of natural and anthropogenic impacts, providing long-term records via various biogeochemical proxies. Sedimentary photosynthetic pigment records can be effectively used to infer both changes in algal composition and lake oxygen conditions (Guilizzoni et al., 1983; Leavitt, 1993; Lami et al., 2000). Chlorophylls, together with their derivatives, and various carotenoids specific to particular groups of algae can be used to reconstruct overall primary production and the composition of past photosynthetic communities (Leavitt and Hodgson, 2001). Pigments such as okenone and isorenieratene, which are specific to phototrophic sulfur bacteria that live in the anoxic sulfidic zones, are regarded as very good indicators of anoxia (Züllig, 1989; Guilizzoni and Lami, 2002). HPLC-inferred pigments have a coarser temporal resolution due to laborious sample preparation and time-consuming HPLC measurements. Scanning Hyperspectral Imaging (HSI), a novel non-destructive method to quantitatively infer the abundance of algal (TChl: chlorophyll $a$ and $b$, and their derivatives) and bacterial pigments (Bphe: bacteriopheophytins $a$ and $b$), offers insight into past trophic and oxygen conditions at unprecedented μm-scale (sub-seasonal) resolution (Butz et al., 2015; Makri et al., 2020), but with lower speciation sensitivity.

In this study, we use the varved sediment record of Lake Jaczno (NE Poland) to explore the specific conditions and mechanisms of trophic and oxygen state changes in the Holocene, under changing climatic and environmental conditions. Our research has been guided by the following questions: i) Which conditions drove algae dynamics and oxygen state changes in the Holocene before any significant human intervention? ii) How did climate, catchment vegetation and erosional input affected the phototrophic community in the lake and iii) How does the current trophic state and mixing regime of the lake compare with the past? For this, we combined a high-resolution HSI-inferred record of TChl and Bphe, X-ray fluorescence (XRF) elemental data, and ~~an HPLC pigment record at coarser resolution~~ a low-resolution pigment record using HPLC analysis with high compound specificity, which cannot be achieved by the HSI record.~~but specific in the analysis.~~ Our dataset was compared with vegetation and temperature reconstruction data to investigate the environmental conditions at times of aquatic primary production and bottom water oxygenation changes. Lake Jaczno provides ideal conditions to answer these questions. It contains an entirely varved Holocene sediment record, which has so far only been analyzed for the last 1700 years for productivity, anoxia (Butz et al., 2016, 2017) and historical land use (Poraj-Górska et al., 2017). Pollen records have revealed that human pressure was low until the 17th century, when landscapes opened and agriculture intensified (Marcisz et al., 2020). ~~This is rare in Europe.~~ Therefore, this site provides a unique opportunity for a long-term Holocene assessment of the natural causes and dynamics of meromixis and hypoxia with limited anthropogenic impact until historic times.

## 2. Study site

Lake Jaczno (54°16'25.5" N 22°52'15.9" E, 163 m a.s.l, Fig. 1a) is a small, 26 m deep, exoreic, kettle-hole lake formed sometime after the Weichselian deglaciation ca. 15 ka BP in the Suwałki Lakeland in NE Poland (Krzywicki, 2002). Lake Jaczno has a total surface area of 0.41 $km^2$ separated in five distinct basins with narrow sills. It is fed by three permanent inflows (N and W) and one outflow in the south (Fig. 1b). Jaczno is classified as dimictic and mesotrophic (Tylmann et al., 2013), with incomplete mixing or possibly even meromixis during some years (Butz et al., 2016). Butz at al. (2017) found that anoxic, and even meromictic conditions, established naturally for most of the past 1700 years. Meromixis was interrupted repeatedly following sediment slumping or flood events.

Microscopic and geochemical analyses in the sediments of Lake Jaczno have revealed seasonal layers (calcareous biogenic varves) with a complex succession of diatoms and calcite, detrital siliciclastic material (quartz, clays), organic fragments, and finally amorphous organic matter (Tylmann et al., 2013; Butz et al., 2016; Poraj-Górska et al., 2017). The lake is surrounded by steep slopes and gullies with ephemeral or perennial water flow, transporting detrital material to the lake (Fig. 1c).

The catchment area (ca. 9 $km^2$) is covered by glacial tills, sands and fluvioglacial deposits. Modern soils are classified as cambisols and podsols in the northern part and ferralic cambisols in the southern part of the catchment. Agricultural lands dominate in the central and northern parts and forests in the southern parts (Fig. 1c). The lake is surrounded by peatlands and forests dominated by birch, alder and spruce (Weisbrodt et al., 2017). The climate of the region is continental with a mean annual temperature of 6.8°C and a mean annual precipitation of 600 mm (IMGW-PIB, 2017). The lakes in the area typically remain ice covered from December to March (Amann et al., 2014).

117 Archeological investigations in the Suwałki region indicate sparse or only seasonal human occupation during the
118 Mesolithic and Neolithic (10,000–3800 cal BP) (Engel and Sobczak, 2012). Around 2000 cal BP human presence
119 increases in the region with stronghold settlements, animal husbandry and fishing (Kinder et al., 2019). Yet, the
120 area around Lake Jaczno remained isolated from human influences (Marcisz et al., 2020). Pollen and charcoal
121 data, and increased soil erosion indicate extensive forest clearance, forest fires and intensified agriculture,
122 suggesting permanent settlements and higher human impact since 500 cal BP, especially after 150 cal BP (1800
123 CE) (Kinder et al., 2019; Marcisz et al., 2020). The 1970s are marked by a regeneration of forest cover and a
124 significant increase of fertilizer use in agriculture (Poraj-Górska et al., 2017; Kinder et al., 2019), which markedly
125 increased lake primary production (Butz et al., 2016; Poraj-Górska et al., 2017).

126 **3.      Materials and methods**

127 Two parallel cores ca. 12.5 m long were retrieved in September 2017, using a UWITEC piston corer. The coring
128 site was located at the deepest part (24 m water depth) of the lake in the southern basin, which is protected from
129 direct external inputs (Fig. 1b). The cores were split lengthwise and then described following Schnurrenberger et
130 al. (2003) and the Munsell color chart (Munsell Color (Firm), 2010). Flood deposits and slumps were identified
131 based on grain size, mineral content, and sediment structure. First, the core halves were analysed using non-
132 destructive methods and further analytical measurements were performed after subsampling. The sampling interval
133 for LOI, CNS and dry-bulk density analysis was 10 cm (ca. 80-year resolution, discrete sampling). For the HPLC
134 and spectrophotometer analysis, 46 discrete samples (1–2 cm$^3$) were taken every ca. 30–35 cm (ca. 230 years
135 resolution) taking into account the HSI scanning data and optimization for the proxy-to-proxy calibration of the
136 HSI indices with spectrophotometer data (Butz et al., 2015). The top 10 cm (last ca. 50 years) were subsampled
137 continuously every 1 cm.
138
139 The chronology is based on 18 radiocarbon Accelerator Mass Spectrometry (AMS) ~~AMS~~ dates on taxonomically
140 identified terrestrial plant macrofossils (Table 1) measured at the Laboratory for Radiocarbon Analysis at the
141 University of Bern. Samples with < 300 μg C were measured using the gas-source input of the MIni CArbon
142 DAting System (Szidat et al., 2014; Zander et al., 2020). The age–depth model was calculated using Bacon (rbacon
143 v. 2.4.2; Blaauw et al., 2020; Blaauw and Christeny, 2011) and the IntCal13 calibration curve (Reimer et al., 2013).
144 Event layers (>3 cm) and slumps were excluded from the age calculation (Fig. 2). According to changes in
145 lithology, we used model parameters that allowed for a higher sedimentation rate in the lowermost 137 cm (Fig.
146 2).
147
148 XRF scanning was performed at continuous 2 mm steps using an ITRAX μXRF core scanner (exposure time 20 s,
149 30 kV and 50 mA) equipped with a Cr-tube at the University of Bern. The results are given as counts (peak area).
150 From the detected elements, Ti was used as proxy for erosional input from the catchment, Ca as a proxy for
151 endogenic calcium carbonates, Si/Ti as a proxy for biogenic silica, S, Fe, Mn, and Mn/Fe as proxies of changing
152 redox conditions (Koinig et al., 2003; Croudace and Rothwell, 2015).
153
154 Hyperspectral imaging scanning (HSI) was performed on the freshly oxidized core halves using a Specim PFD-
155 CL-65-V10E camera (400 to 1000 nm spectral range; 2.8 nm spectral resolution). We used a spatial resolution of
156 ~68 μm per pixel with a spectral sampling of 1.57 nm. Data were processed using the ENVI software version 5.4

157  (Exelis Visual Information Solutions, Boulder, Colorado) following Butz et al. (2015). The relative absorption

158  band depths (RABDs) were calculated based on spectral endmembers analysis in ENVI. The $RABD_{673}$ (spectral

159  region 590–730 nm) was used to detect chlorophyll *a and b*s and their diagenetic products (TChl) and served as a

160  proxy for aquatic primary production (Leavitt and Hodgson, 2001). The $RABD_{845}$ (spectral region 790–895 nm)

161  was used to detect total bacteriopheophytin *a* and *b* (*Bphe*) (Butz et al., 2015, 2016), which is a proxy for anoxia

162  and meromixis as described in Makri et al. (2020). Bphe *a* and *b* is produced by anoxygenic phototrophic purple

163  sulfur and non-sulfur bacteria that proliferate in illuminated anoxic habitats (Yurkov and Beatty, 1998; Madigan

164  and Jung, 2009). Green sulfur bacteria produce bacteriochlorophyll *c*, *d* and *e*, which do not absorb in the $RABD_{845}$

165  range. Therefore, HSI-inferred Bphe reflects purple bacteria abundance.

166

167  The spectral indices were calibrated with absolute pigment concentrations of 46 selected sediment samples (1 $cm^3$)

168  measured by spectrophotometry (Shimadzu UV-1800). Pigments were extracted using pure acetone. The

169  supernatant was evaporated under nitrogen, and extracts were subsequently redissolved in 2 ml of pure acetone

170  (method adapted from Schneider at al. 2018). For the calculation of Bphe concentrations, we used the molar

171  extinction coefficient for Bphe *a* by Fiedor et al. (2002). For TChl, we applied the molar extinction coefficient for

172  chlorophylls and chlorophyll derivatives by Jeffrey et al. (1975). The performance of the proxy-to-proxy linear

173  regression models was assessed using the coefficient of determination ($R^2$) and the root mean square error of

174  prediction (RMSEP) (Butz et al., 2015) run in R (R Core Team, 2015). The calibration model for TChl showed an

175  $R^2$ of 0.91 ($p < 0.001$) and a RMSEP ~8 % (Fig. S1a). The calibration model for Bphe showed an $R^2$ of 0.95 ($p <$

176  0.001) and a RMSEP ~6 % (Fig. S1b). The Shapiro–Wilk and the Kolmogorov–Smirnov tests of the residuals

177  show that they are most likely normally distributed, suggesting that inferences can be made with both models.

178

179  HPLC analysis was conducted on the same 46 samples used for the proxy-to-proxy calibration. Chlorophyll,

180  chlorophyll derivatives and carotenoids were measured using ion pairing reverse-phase (Mantoura and Llewellyn,

181  1983; Hurley, 1988). The system used a UV-VIS detector set at 460 nm and 656 nm for carotenoids and

182  chloropigments, respectively. The results were corrected for water content and expressed as nmol g $OM^{-1}$ (Züllig,

183  1982; Guilizzoni et al., 1983; Lami et al., 1994). According to Jeffrey et al. (2011), Guilizzoni and Lami (2002),

184  chlorophyll *a*, *ββ*-carotene, pheophytin *a*, and pheophytin *b* are considered as indicators of total algal biomass.

185  Chlorophyll *b* and lutein are associated with green algae. *B*-carotene, dinoxanthin (pyrophytes), diadinoxanthin

186  (siliceous algae), fucoxanthin (diatoms), diatoxanthin (chrysophytes) and alloxanthin (cryptophytes) are related to

187  brown algae. Echinenone and zeaxanthin are associated to most taxa of blue–green algae, and myxoxanthophyll

188  and canthaxanthin to colonial and filamentous cyanobacteria (Leavitt and Hodgson, 2001). K-myxol (4-keto-

189  myxol-2'-methylpentoside) is associated with N-fixing cyanobacteria (*Anabaena flos-aquae*) (Kosourov et al.,

190  2016). Pheophorbide *a* is a degradation product of Chl *a* transformed by microbial processes and used as

191  considered asan indicator of grazing (Bianchi and Findlay, 1991; Cartaxana et al., 2003). In the phototrophic

192  bacteria community, BChl *a* is common to all anoxygenic phototrophic purple bacteria. Okenone (*Chromatium*

193  *sp.*) is associated with purple sulfur bacteria (PSB), whereas spheroidene and spheroidenone (*Rhodopseudomonas*

194  *sphaeroides*) are related to purple nonsulfur bacteria (PnSB). Both groups are able to oxidize sulfide. Yet, PSB

195  store any $S^0$ formed intracellularly, whereas PnSB do so outside the cell (Madigan and Jung, 2009). The main

196  difference between the two groups is that PSB are strong photoautotrophs, whereas PnSB are physiologically

197  versatile and can grow well both phototrophically and in darkness via fermentation or anaerobic respiration

198  (Madigan and Jung, 2009). *R. sphaeroides* are also excellent N-fixing bacteria. Oxygen tolerance varies among

199  species, with *R. sphaeroides* being able to grow under vigorous aeration. Spheroidenone is produced by *R.

200  sphaeroides* only when even small amounts of oxygen are present (Züllig, 1989). Hence, the presence of

201  spheroidenone is used as an indication of better oxygen conditions, whereas the presence of spheroidene with

202  parallel absence of spheroidenone is used as an indication of meromictic conditions (Züllig, 1989; Guilizzoni and

203  Lami, 2002). Isorenieratene is associated with GSB (*Chlorobium sp.*). GSB have low light requirements and can

204  cope with low light availability, occupying deeper layers in stratified lakes (Montesinos et al., 1983). Hence, a

205  dominance of GSB over PSB is used as an indicator of a deeper oxic–anoxic boundary (Montesinos et al., 1983;

206  Itoh et al., 2003).

207

208  Total organic carbon (TOC) was determined by Loss on Ignition (LOI; Heiri et al., 2001). Total carbon (TC) and

209  total nitrogen (TN) were measured with a CNS-Analyzer (Elementar vario EL cube). Total inorganic carbon (TIC)

210  was calculated by the difference between TC and TOC (Enters et al., 2010). The TOC/TN ratio was used to infer

211  changes in OM sources (Meyers, 2003). The lithogenic flux was calculated based on the residual calculation after

212  removing the organic matter and carbonate fraction by LOI.

213

214  Statistical analysis was performed in R (R Core Team, 2015). To define the sedimentary lithotypes we performed

215  an hierarchical unconstrained clustering on the geochemical proxies (XRF data: Ti, Ca, Si/Ti, Si, S, Fe, Mn, Mn/Fe;

216  HSI: TChl, Bphe; TOC, TIC, TN, TOC/TN, Fig. 3) using the Euclidean distance matrix and the ward.D2 clustering

217  method (Murtagh and Legendre, 2014). On the same dataset, we performed a PCA analysis with the samples

218  grouped based on the unconstrained clustering to investigate the relationships between the lithotypes and the

219  geochemical variables (Fig. S2). The data were log transformed and scaled before statistical analysis. We

220  performed a redundancy analysis (RDA) using the Vegan package (Oksanen et al., 2016) in R to relate the pigment

221  matrix i.e HPLC- and HSI-inferred pigment concentrations (Hellinger-transformed variables) to the environmental

222  variables i.e. temperature (Heikkilä and Seppä, 2010), arboreal pollen (AP), non-arboreal pollen (NAP) (Kinder et

223  al., 2019; Marcisz et al., 2020) and lithogenic flux (log transformed variables). The elements were plotted using

224  scaling 2 (see Borcard et al., 2011, pp. 166–167). This analysis was followed by a permutation test in R to test for

225  significance in the redundancy analysis (Legendre and Legendre, 1998; Borcard et al., 2011). The zones of pigment

226  data were defined by constrained clustering using the Bray distance and ward.D2 linkage method in R.

227  **4.      Results and interpretation**

228  **4.1     Chronology**

229  The age–depth model (Fig. 2) reveals a basal age of ca. 9500 cal BP. The model shows a stationary distribution,

230  matching prior and posterior accumulation rates, and a smooth sediment accumulation as indicated by its memory

231  or variability (Fig. 2). Three radiocarbon samples (Fig. 2, in red) have calibrated ages that do not fit with the 95 %

232  confidence interval. Based on the lithology and the much older ages, these samples were considered as containing

233  reworked carbon and were excluded from the Bacon model. The sediment sequence is entirely laminated

234  throughout the Holocene showing regular continuous sedimentation without any hiatus. In the lowermost section

235  (1257–1120 cm), sedimentation rates (SR) are relatively high (0.5 cm $y^{-1}$) and the mean age error (95% confidence

236  interval) is ca. ±160 years. Numerous event layers and slumps characterize the part between 1120 cm and 800 cm

237 where the SR is ca. 0.2 cm $y^{-1}$ and the mean age error is ca. ±200 years. From 800 cm to the top, the sediment is

238 continuously varved and the SR is 0.1 cm $y^{-1}$ (0.2 cm $y^{-1}$ in the last 500 years). The mean age error in this section

239 is ca. ±140 years. The ages at the top 10 cm of the core (data shown in Fig 4b) were calculated by extrapolation of

240 the radiocarbon chronology to the sediment surface. A stratigraphic correlation with the ^{210}Pb dated cores from

241 Butz et al. (2016) showed an age error of ±5 years for this section.

## 4.2    Lithotypes and biogeochemical proxies

243 Figure 3 shows the biogeochemical data that defined four sedimentary lithotypes A–D. Fig. S3 (supplementary

244 material) shows the RGB images and the biogeochemical composition of selected close-ups within the sediment

245 sequence. Lithotype A and B appear in segments between ca. 9500–6800 cal BP (Fig. 3). Lithotype A, at the

246 bottom part (9500–9200 cal BP), consists of light greenish grey (GLEY 2 7/2) fine sand and continues with pale

247 yellow (2.5Y 7/3) and grey (2.5Y 5/1) laminations with light greenish grey silty lenticular bedding. This part is

248 characterized by high detrital inputs (Ti, lithogenic flux), moderate carbonate content (Ca, TIC), low production

249 and biogenic silica (HSI-TChl, Si/Ti) and low TOC. Low HSI-Bphe and S, and higher Mn/Fe ratio indicate

250 effective oxygenation of bottom waters. From ca. 9200–8500 cal BP, lithotype B is introduced and is characterized

251 by slightly higher production (HSI-TChl) and biogenic silica (Si/Ti); carbonates (TIC, Ca), TOC and TN contents

252 increase, whereas higher S, Fe and HSI-Bphe, and lower Mn/Fe ratio indicate the development of anoxic (sulfidic)

253 conditions. Between ca. 8500–6800 cal BP, lithotype A continues with varved sediments; starting with biogenic

254 pale yellow (2.5Y 7/3) and grey (2.5Y 5/1) varves with intercalated reddish brown (2.5YR 5/4) and reddish black

255 (2.5YR 2.5/1) laminations rich in clastic material and iron oxides. In the second half of this part, varves are less

256 well-preserved with several intercalated clastic-rich laminations. Based on color, layer thickness, and grain size

257 we interpret these intercalated layers as event (flood) deposits. In this period, lithotype A is characterized by high

258 detrital input (Ti, lithogenic flux); primary production (HSI-TChl) remains unchanged and carbonates (Ca, TIC)

259 show increased variability. Biogenic silica (Si/Ti), TOC and Fe slightly decrease. S decreases, HSI-Bphe is very

260 low or absent and Mn/Fe increases, suggesting better oxygen conditions.

262 Lithotype C occurs between ca. 6800–500 cal BP and consists mainly of light grey (2.5YR) and dark grey (2.5YR

263 4/1) fine biogenic varves, with some dispersed event layers that occur only at the beginning of this period until ca.

264 6000 cal BP. This period is characterized by low erosional input (Ti, lithogenic flux), gradually increasing

265 production (HSI-TChl) and TOC content, fluctuating biogenic silica (Si/Ti) and constantly high carbonates content

266 (Ca, TIC). S counts are minimal. HSI-Bphe is mostly present suggesting the development of anoxic conditions in

267 the hypolimnion. Mn/Fe seems to fluctuate, with higher values when HSI-Bphe is lower and vice versa.

269 Lithotype D occurs from ca. 500 cal BP to the present and consists of biogenic pale yellow (2.5Y 7/3), grey (2.5Y

270 5/1) and dark grey (2.5Y 4/1) calcareous biogenic varves. This period is characterized by instances of higher

271 detrital input (Ti) and several intercalated event (flood) layers. Mn counts also increase. Primary production (HSI-

272 TChl), TOC and TN reach maximum levels, whereas biogenic silica and carbonates (Ca, TIC) decrease. HSI-Bphe

273 reach maximum values at the top suggesting persistent anoxia in this part. The Mn/Fe ratio and HSI-Bphe show

274 opposite fluctuations indicating phases of better oxygen conditions when Bphe is absent.

### 4.3    HPLC pigment stratigraphy

Figure 4 presents the pigment dataset of individual chlorophylls and carotenoids measured by HPLC in the Holocene (Fig. 4a), and for the last 50 years (Fig. 4b). The pigments are grouped according to their taxonomic relation and the zones are defined by constrained clustering, which yielded boundaries that are similar to those of the sediment lithotypes (Fig. 3).

In zone I (ca. 9500–9200 cal BP), pigment concentrations are very low. Chromophytes are more abundant than green algae, especially cryptophytes (alloxanthin) and chrysophytes (fucoxanthin). Blue–green algae (echinenone, zeaxanthin) are present in low concentrations. Grazing (pheophorbide *a*) is low. In the purple bacteria group, *Chromatium* species (okenone, PSB) are absent, whereas *R. sphaeroides* (spheroidene and spheroidenone, PnSB) are both present in low concentrations. *Chlorobium sp.* (isorenieratene, GSB) are present in traces.

In zone II (ca. 9200–6700 cal BP), pigment concentrations increase overall. Green algae (chlorophyll *b*, lutein) still have low concentrations, whereas chromophytes (*β*-carotene) become more abundant especially pyrophytes (dinoxanthin) and chrysophytes (diatoxanthin) that show a distinctive local maximum around 7300 cal BP. Colonial filamentous cyanobacteria (canthaxanthin) appear in this zone. Grazing (pheophorbide *a*) starts increasing around 8300 cal BP. *Chromatium sp.* (okenone, PSB) is mostly absent. *R. sphaeroides* (spheroidene and spheroidenone, PnSB) have moderate concentrations, whereas *Chlorobium sp.* (isorenieratene, GSB) reach a maximum around 7300 cal BP.

In zone III (6700–500 cal BP), most pigments concentration increase gradually. Green algae (chlorophyll *b*) increase significantly. Chromophytes remain abundant. Diatoms and other siliceous algae (diadinoxanthin, fucoxanthin), and cryptophytes (alloxanthin) show a local maximum around 2000 cal BP. Blue–green algae (echinenone, zeaxanthin) increase gradually. More colonial filamentous cyanobacteria (myxoxanthophyll) appear around 2300 cal BP and, together with zeaxanthin, reach a maximum around 2000 cal BP. N-fixing cyanobacteria (k-myxol) appear at ca. 5000 cal BP. *Chromatium sp.* (okenone, PSB) appear in this zone and increase gradually. *R. sphaeroides* (spheroidene and spheroidenone, PnSB) also show a gradual increase, whereas *Chlorobium sp.* (isorenieratene, GSB) decrease to minimum concentrations.

Zone IV (500 cal BP to present), is characterized by a further gradual increase of most pigments, reaching unprecedented maximum concentrations at the top. In more detail, Fig. 4b shows the distribution of pigment concentrations in the last 50 years. Most pigments reach maximum values around 1997 CE. *Chromatium sp.* (okenone, PSB) have high concentrations, whereas *R. sphaeroides* are present producing only spheroidene and almost no spheroidenone. *Chlorobium sp.* (isorenieratene, GSB) show only trace concentrations around 1997 CE.

### 4.4    The relationships between land use, temperature, and pigment stratigraphy

We applied a redundancy analysis (RDA) to examine the response of our HPLC- and HSI-inferred pigment dataset to land use changes (arboreal pollen: AP, and non-arboreal pollen: NAP; Kinder et al., 2019; Marcisz et al., 2020), annual mean temperature variability (Heikkilä and Seppä, 2010) and catchment surface processes (lithogenic flux). Figure 5 shows the RDA ordination output in a triplot with the explanatory variables (in blue) and response (in red) variables, as well as the samples divided into the four distinct zones defined by constrained clustering (see

315 Sect. 4.3). The numerical output shows that the first two axis (RDA 1 20.95 % and RDA 2 11.25 %) explain 36 %

316 of the variation (unadjusted values). The $R^2_{adj}$ for the constrained ordinations suggests that this model explains ca.

317 29 % of the variation in the data. The permutation test on the unconstrained ordinations indicates that the first two

318 axis are significant (p<0.001; Table S1) and represent the data adequately.

319

320 The RDA triplot (Fig. 5) shows that AP and NAP play an important role in the distribution of the pigment data

321 along the first axis (RDA 1). Lithogenic flux and temperature drive pigment variability along the second axis

322 (RDA 2). Lithogenic flux is strongly correlated with siliceous algae (fucoxanthin, diadinoxanthin) and blue–green

323 algae (echinenone), as well as enhanced aquatic primary production (HSI-TChl) by green algae (lutein) and

324 cryptophytes (alloxanthin, $\beta$-carotene). Lithogenic flux is clearly anticorrelated with PSB (okenone, HSI-Bphe)

325 and Chl $a$. AP is mainly correlated with GSB pigments (isorenieratene) indicating a deeper oxic–anoxic boundary,

326 and PnSB (spheroidene and spheroidenone) that suggest a more effective oxygenation of the water column. AP is

327 also correlated with variables indicating the presence of chromophyte (brown) algae, pyrophytes (dinoxanthin),

328 chrysophytes (diatoxanthin), as well as some blue–green algae (zeaxanthin). Higher lithogenic input and AP drive

329 pigment variability in zones I and II. Temperature seems to be correlated with higher production of some green

330 algae (Chl $b$, pheophytin $b$), increased cyanobacteria abundance ($\beta\beta$-carotene, $\beta$-carotene) and colonial-

331 filamentous cyanobacteria (myxoxanthophyll, canthaxanthin). Temperature seems to drive pigment variability

332 mainly in zone III. NAP is correlated with PSB production (BChl $a$, HSI-Bphe and okenone), overall higher

333 primary production (Chl $a$, pheophytin $a$), higher grazing (pheophorbide $a$), and N-fixing cyanobacteria (k-myxol).

334 NAP drives pigment variability in zone IV.

335 **5.    Discussion**

336 **5.1     Combining sedimentological and biogeochemical data to infer past lake production and bottom**
337 **water oxygenation**

338 The 12.5 m long and almost entirely varved sediment record of Lake Jaczno continuously spans the last ca. 9500

339 cal yr BP (Fig. 2). The chronology is robust and exclusively based on terrestrial macrofossils. The lithology of

340 Lake Jaczno (Fig. 3) revealed the deposition of frequent event layers between 8500–7000 cal BP, which likely

341 reflect a regional catchment/climatic signal as similar features have been observed, for the same period, in the

342 nearby Lake Szurpiły (Kinder et al., 2020). The physical characteristics of the catchment favored the transport of

343 lithogenic material into the lake (Fig. 3), thereby possibly affecting the density stratification, light availability, and

344 subsequently the phototrophic community dynamics. A proper assessment of these changes requires high-

345 resolution data that is impossible to reach using HPLC data alone. Yet, the combination of high-resolution (μm-

346 scale) calibrated HSI bulk data for TChl and Bphe, combined with scanning XRF and compound specific HPLC

347 data, provides a unique opportunity for paleoproduction and paleooxygenation reconstructions at sub-seasonal

348 scale for multi-millennial-long records (Butz et al., 2017; Makri et al., 2020). This approach is directly applicable

349 to diverse lacustrine (Butz et al., 2017; Schneider et al., 2018; Makri et al., 2020; Sanchini et al., 2020) and

350 potentially marine environments (Hubas et al., 2011, 2013) with uncertain past redox state changes.

351

352 The calibration of the $RABD_{673}$ and $RABD_{845}$ to absolute pigment concentrations of green pigments (chlorophylls

353 and diagenetic products) and Bphe ($a$ and $b$) respectively, revealed robust calibration statistics (Fig. S1,

354 supplementary material) with very low uncertainties (ca. 6–8 %) comparable to other studies (Butz et al., 2017;

Schneider et al., 2018; Makri et al., 2020; Sanchini et al., 2020). Between ca. 9200 and 7000 cal BP, the calibration model of the $RABD_{673}$ for green pigments calculates negative concentrations (Fig. 3). This offset can be produced by matrix effects, i.e. the variability of the reflectance of the sediment matrix or substances that absorb in the same range as chlorophylls and their diagenetic products (590–730 nm) (Makri et al., 2020). Interestingly, GSB (isorenieratene) peak between 9200 and 7000 cal BP (Fig. 4). GSB contain bacteriochlorophyll *c*, *d*, and *e* that absorb in the same range as chlorophylls and chlorophyll derivatives (Oren, 2011). This could indicate that a part of the $RABD_{673}$ calibration error may be due to the increased GSB abundance. Nonetheless, the calibration statistics reveal an overall error of less than 8 %.

## 5.2 Holocene production dynamics and chemocline evolution

The presence of anoxygenic sulfur bacteria throughout our record, combined with chlorophylls, carotenoids and geochemical evidence, suggests that euxinic conditions prevailed in Lake Jaczno for most of the past 9500 years. Nonetheless, the changing composition of photosynthetic sulfur bacteria indicates persisting but variable euxinia. Figure 6 summarizes the Holocene evolution of the relative abundance of PSB, PnSB and GSB, *Chromatium* (okenone) and *Clorobium* (isorenieratene), the content of spheroidene and spheroidenone pigments produced by *R. sphaeroides*, and the high-resolution calibrated HSI-TChl and Bphe, with respect to lithogenic flux, climate variability (annual mean temperature; Heikkilä and Seppä, 2010) and human impact (land use and vegetation cover; Kinder et al., 2019; Marcisz et al., 2020).

### 5.2.1 Low trophic levels with a deep oxic–anoxic boundary

In the period from 9500 to 6700 cal BP, which corresponds to pigment zones I and II, the phototrophic bacteria population is dominated by GSB (Fig. 6). A small percentage of PnSB (*R. sphaeroides*) is present and seems to produce both spheroidene and spheroidenone during this time. *Chromatium* (okenone, PSB) is almost completely absent. Considering that *R. sphaeroides* produces spheroidenone only when even small amounts of oxygen is present (Züllig, 1989) we suggest that, in this period, euxinic conditions were already present but the strength or extent of anoxia was likely weak. HSI-Bphe that corresponds to purple bacteria is very low. Anoxia is mainly a function of lake stratification and productivity. HSI-TChl, which indicates total primary production, is still at low levels (Fig. 6). Indeed, the stratigraphy of individual pigments indicates low to moderate in-lake production, which mainly consists of chromophyte (brown) algae and some colonial cyanobacteria (canthaxanthin) (Fig. 4), which is also confirmed in the RDA analysis (Fig. 5). Brown siliceous algae are well adapted and tolerant algae species that thrive in oligotrophic conditions in symbiosis with other algae species and bacteria (Bird and Kalff, 1986; Wetzel, 2001). Similar observations of algae composition were made in Lake Peipsi (Tõnno et al., 2019; Estonia) and Lake Lazduny (Sanchini et al., 2020; NE Poland).

Temperature gradually increased and a closed forest canopy with pine/birch and later elm/hazel/alder persisted in the catchment (Fig. 6) (Gałka, 2014). These provided shelter from wind and increased the nutrient pools in the catchment soils (Bajard et al., 2017). The closed forest canopy, combined with the deep and relatively small basin (relative depth 3.01 %), favors the establishment of a naturally anoxic hypolimnion (Zolitschka et al., 2015). Yet, it seems that enhanced permanent stratification was still not established in the lake. This phase of GSB dominance corresponds to a period of high lithogenic flux or high-energy sedimentation (Fig. 3, 6), as confirmed in the RDA analysis (Fig. 5). Turbidity currents and underflows can increase turbidity and nutrient availability, but can also

394  cause sporadic ventilation of bottom waters. Higher suspended matter and/or algal growth would decrease light
395  availability in the oxic–anoxic boundary. Since GSB and PnSB are more tolerant to low light intensities than PSB
396  (Biebl and Pfennig, 1978; Parkin and Brock, 1980; Madigan and Jung, 2009), a dominance of GSB and presence
397  of spheroidene and spheroidenone in the sediments is expected under these conditions. Similar observations were
398  made in Lake Cadagno (Wirth et al., 2013). GSB often inhabit the lowermost part of stratified water bodies due to
399  their efficient light capture (Manske et al., 2005; Imhoff, 2014). Higher abundance of GSB could also indicate a
400  deep oxic–anoxic boundary in the lake (Itoh et al., 2003; Antoniades et al., 2009).

401  ### 5.2.2  Gradually increasing trophy levels with a shallower oxic–anoxic boundary

402  The period from 6700 to 500 cal BP, which corresponds to pigment zone III, is characterized by a gradual shift in
403  the phototrophic bacterial community to higher PSB abundance, especially after ca. 2000 cal BP (Fig. 6). GSB are
404  present, inhabiting the anoxic layers below PSB and seem to fluctuate as a function of the primary production in
405  the oxic layer (HSI-TChl) and related light availability (Montesinos et al., 1983). When production was higher in
406  the oxic layers, *Chromatium* (okenone, PSB) increased and *Chlorobium* (isorenieratene, GSB) decreased. This is
407  also confirmed by the individual pigment stratigraphy (Fig. 4). Green algae (chlorophyll *b*, lutein) and N-fixing
408  cyanobacteria (k-myxol) increase markedly since ca. 5500 cal BP, indicating a higher lake trophy than before,
409  driven most probably by lake ontogeny and a gradual increase of nutrient availability. The appearance of N-fixing
410  cyanobacteria at that time agrees with this interpretation. Prolonged periods of anoxia leading to intense recycling
411  of phosphorous from the sediments would decrease the N:P ratio in the water column promoting nitrogen fixation
412  by N-fixing algae (Howarth et al., 1999; Vitousek et al., 2002). Similar trends in lake trophy evolution are reported
413  from nearby Lake Szurpiły (Kinder et al., 2019) and Lakes Albano and Peipsi (Lami et al., 2000; Guilizzoni and
414  Lami, 2002; Tõnno et al., 2019). An increase of *Chromatium* (okenone, PSB) over *Chlorobium* (isorenieratene,
415  GSB) with increasing lake trophy has been reported from other lakes, e.g. Lake Albano in Italy (Lami et al., 1994),
416  Little Round Lake in Canada (Brown et al., 1984), and Lake Hamana in Japan (Itoh et al., 2003). *R. sphaeroides*
417  (PnSB) are also present producing both spheroidene and spheroidenone, suggesting phases of effective aeration of
418  bottom waters (Züllig, 1989).
419
420  The catchment is continuously densely forested and human impact is very low (Fig. 6). The RDA analysis points
421  to a temperature driven pigment variability in this zone, but mainly for cyanobacteria abundance (Fig. 5).
422  Cyanobacteria can benefit from higher water temperature, yet nutrient inputs have in most cases a much stronger
423  and synergetic effect (Lürling et al., 2018). Temperature variability did not seem to have affected lake stratification
424  directly. However, seasonality, precipitation and windiness play an important role in lake circulation and are not
425  reflected in the annual mean temperature variability. Hence, the role of climate may be underestimated. The oxic–
426  anoxic stratification was enhanced in this period but permanent perennial anoxia was still not established as
427  indicated also by the low HSI-Bphe concentrations. The increase in PSB abundance suggests a shallower oxic–
428  anoxic boundary (Itoh et al., 2003). It appears that during most of the Holocene, anoxia was largely influenced by
429  primary production and lithogenic flux. The case of Lake Jaczno is different from e.g Lake Łazduny (Masurian
430  Lake District, NE Poland; Sanchini et al., 2020), where erosional input is negligible and anoxia was mainly a
431  function of primary production and forest cover.

### 5.2.3    20th century eutrophication, shallow oxic–anoxic boundary and meromixis

In the period from 500 cal BP to the present, which corresponds to pigment zone I, phototrophic sulfur bacteria composition changed to an almost complete dominance of purple bacteria (Fig. 6). Between 500–200 cal BP, HSI-Bphe and the absolute concentrations of PSB (okenone,) and PnSB (spheroidene and spheroidenone) are at a minimum, but dominate the phototrophic bacteria community since GSB are completely absent (Fig. 4, 6). Lake production (HSI-TChl) also decreases while lithogenic flux increases (Fig. 6). These suggest an oxic rather than anoxic phase during this period, with some intervals of weak euxinia. Increased Mn accumulation during this time (Fig. 3) supports the indications of rather oxygenated bottom waters.

Between 200 cal BP to the present, when human impact starts to increase in the catchment (Fig. 5), PSB increase as well. Presence of spheroidene and only trace concentrations of spheroidenone (PnSB) and isorenieratene (GSB) suggest increasing and gradually persisting anoxia. Intensive agriculture in the last 100 years and and use of fertilizers, combined with exceptionally warm summers after 1990 CE (Czernecki and Miętus, 2017; IMGW-PIB, 2017) increased primary production (HSI-TChl) substantially to unprecedented levels in the 1990s, relative to the Holocene baseline. This is also reflected in the individual pigment stratigraphy (Fig. 4). Bphe reaches maximum levels suggesting persisting anoxia and mostly meromictic conditions in the lake, especially since the 1970s when gradual afforestation in the catchment is observed. This is also supported by the HPLC-inferred composition of phototrophic bacteria (Fig. 3).

In this period, the high-resolution HSI-Bphe record indicates that the intervals of lowest AP in the catchment coincide with absence of Bphe, indicating oxic bottom waters. Bphe increases again only when AP and the tree canopy recovers (Fig. 6), with a parallel absence of spheroidenone (PnSB), suggesting meromictic conditions. Butz et al. (Butz et al., 2016, 2017) showed that these intervals of low AP and low or absent Bphe in the sediments were accompanied by strong pulses of terrigenous material from the catchment. The role of human impact with regard to anoxia and interrelated catchment processes (deforestation/afforestation and nutrient inputs) has also been shown in other lakes with diverse timing of human impact onset. For example, Lake Moossee (Makri et al., 2020) and Soppensee (Lotter, 1999) on the Swiss Plateau, Lakes Albano and Nemi in Italy (Guilizzoni et al., 2002), Lake Zazari in Greece (Gassner et al., 2020) with an early Mid-Holocene human impact, and Lake Szurpiły (Kinder et al., 2019) in the vicinity of Lake Jaczno with a late human impact, mainly in the last 500 years.

### 6.    Conclusions

In this study, we used a multiproxy approach, combining high-resolution HSI pigment data with lower resolution HPLC-inferred concentrations of specific algal pigments, and geochemical data to investigate algal community composition and its relationship with aquatic production and water column oxygenation in a 9500-years sediment record from NE Poland. Land use changes, vegetation cover and climate variability were also taken into account. Our aim was to examine factors that determine trophic state changes and lake stratification, in a lake system with stable catchment vegetation and low human impact until very recent times.

The Holocene sedimentary pigment and geochemical record of Lake Jaczno revealed distinct changes in lake trophy and stratification states, mainly driven by the catchment evolution, lithogenic flux, nutrient input and subsequent increase in primary production. The lake had a first phase (9500–6700 cal BP) of low production that

consisted mainly of brown algae in the oxic zone, yet an early immediate establishment of weak euxinic conditions in a deep water column dominated by GSB in its anoxic zone. Increased suspended loads, turbidity currents and underflows seem to have increased turbidity and restricted the proliferation of PSB at the deep oxic–anoxic boundary. Between 6700–500 cal BP, primary production increased gradually with higher contributions of green algae and cyanobacteria, following lake ontogeny in a continuously densely forested catchment. The oxic–anoxic boundary became gradually shallower with a shift from GSB to PSB. The composition of phototrophic bacteria and the presence of spheroidene and spheroidenone (PnSB) in the sediments suggest pronounced yet intermittent euxinia in the lake. Between 500 cal BP to the present, lake trophy increases dramatically, especially in the last 100 years, due to intensified human impact. Eutrophication accompanied by catchment deforestation and subsequent afforestation after land abandonment were the main driving forces for the establishment of permanently anoxic and meromictic conditions in the modern lake.

This study highlights the great potential of calibrated and validated HSI measurements combined with HPLC data. Lake Jaczno provided a rare site to explore the mechanisms that can potentially induce changes in lake mixing, production and sustained bottom water anoxia in times from minimum to intensive human impact, in a naturally stratified lake system. Our findings, together with findings from other lakes across Europe, can greatly expand our understanding on these major environmental problems while providing a tailored toolset for implementing effective remediation techniques in the future.

**Data availability**

The data will be madeis available at PANGAEA BORIS https://doi.org/10.5194/bg-2020-362.

**Author contributions**

**Stamatina Makri**: Investigation, Data Curation, Formal analysis, Writing - Original Draft, Visualization. **Luyao Tu:** Investigation, Writing - Review & Editing. **Andrea Lami:** Investigation, Writing - Review & Editing. **Wojciech Tylmann:** Writing - Review & Editing. **Hendrik Vogel:** Writing - Review & Editing, **Martin Grosjean:** Conceptualization, Methodology, Writing - Review & Editing, Supervision, Funding acquisition.

**Competing interests**

The authors declare that they have no conflict of interest.

**Acknowledgments**

This study was funded by the Hans Sigrist Stiftung and the Swiss National Science Foundation Grants (SNF 200021_172586). We thank Andre F. Lotter, Willi Tanner, Paul Zander and Maurycy J Żarczyński for their help during field work. We thank Petra Boltshauser-Kaltenrieder for plant macrofossils identification. Further, we acknowledge Daniela Fischer and Patrick Neuhaus for their assistance in the lab.

**References**

Adrian, R., O'Reilly, C. M., Zagarese, H., Baines, S. B., Hessen, D. O., Keller, W., Livingstone, D. M., Sommaruga, R., Straile, D., Van Donk, E., Weyhenmeyer, G. A. and Winder, M.: Lakes as sentinels of climate change, Limnol. Oceanogr., 54(6 PART 2), 2283–2297, doi:10.4319/lo.2009.54.6_part_2.2283, 2009.

Amann, B., Lobsiger, S., Fischer, D., Tylmann, W., Bonk, A., Filipiak, J. and Grosjean, M.: Spring temperature variability and eutrophication history inferred from sedimentary pigments in the varved sediments of Lake Zabińskie, north-eastern Poland, AD 1907-2008, Glob. Planet. Change, 123(PA), 86–96, doi:10.1016/j.gloplacha.2014.10.008, 2014.

Antoniades, D., Veillette, J., Martineau, M. J., Belzile, C., Tomkins, J., Pienitz, R., Lamoureux, S. and Vincent, W. F.: Bacterial dominance of phototrophic communities in a High Arctic lake and its implications for paleoclimate analysis, Polar Sci., 3(3), 147–161, doi:10.1016/j.polar.2009.05.002, 2009.

Bajard, M., Poulenard, J., Sabatier, P., Develle, A. L., Giguet-Covex, C., Jacob, J., Crouzet, C., David, F., Pignol, C. and Arnaud, F.: Progressive and regressive soil evolution phases in the Anthropocene, Catena, 150, 39–52, doi:10.1016/j.catena.2016.11.001, 2017.

Battarbee, R. W. and Bennion, H.: Using palaeolimnological and limnological data to reconstruct the recent history of European lake ecosystems: introduction, Freshw. Biol., 57(10), 1979–1985, doi:10.1111/j.1365-2427.2012.02857.x, 2012.

Bennion, H. and Simpson, G. L.: The use of diatom records to establish reference conditions for UK lakes subject to eutrophication, J. Paleolimnol., 45(4), 469–488, doi:10.1007/s10933-010-9422-8, 2011.

Bianchi, T. S. and Findlay, S.: Decomposition of Hudson estuary macrophytes: Photosynthetic pigment transformations and decay constants, Estuaries, 14(1), 65–73, doi:10.2307/1351983, 1991.

Biebl, H. and Pfennig, N.: Growth yields of green sulfur bacteria in mixed cultures with sulfur and sulfate reducing bacteria, Arch. Microbiol., 117(1), 9–16, doi:10.1007/BF00689344, 1978.

Bird, D. F. and Kalff, J.: Bacterial Grazing by Planktonic Lake Algae, Science (80-. )., 231(4737), 493–495, doi:10.1126/science.231.4737.493, 1986.

Blaauw, M. and Christeny, J. A.: Flexible paleoclimate age-depth models using an autoregressive gamma process, Bayesian Anal., 6(3), 457–474, doi:10.1214/11-BA618, 2011.

Blaauw, M., Christen, J. A., A. Aquino L., M., Esquivel Vazquez, J., Gonzalez V., O. M., Belding, T., Theiler, J., Gough, B. and Karney, C.: Age-Depth Modelling using Bayesian Statistics, 2020.

Borcard, D., Gillet, F., Legendre, P., Borcard, D., Gillet, F. and Legendre, P.: Canonical Ordination, in Numerical Ecology with R, pp. 153–225, Springer, New York, NY., 2011.

Brown, S. R., McIntosh, H. J. and Smol, J. P.: Recent paleolimnology of a meromictic lake: Fossil pigments of photosynthetic bacteria, SIL Proceedings, 1922-2010, 22(3), 1357–1360, doi:10.1080/03680770.1983.11897499, 1984.

Butz, C., Grosjean, M., Fischer, D., Wunderle, S., Tylmann, W. and Rein, B.: Hyperspectral imaging spectroscopy: a promising method for the biogeochemical analysis of lake sediments, J. Appl. Remote Sens., 9(1), 096031, doi:10.1117/1.JRS.9.096031, 2015.

Butz, C., Grosjean, M., Poraj-Górska, A., Enters, D. and Tylmann, W.: Sedimentary Bacteriopheophytin a as an indicator of meromixis in varved lake sediments of Lake Jaczno, north-east Poland, CE 1891–2010, Glob. Planet. Change, 144, 109–118, doi:10.1016/j.gloplacha.2016.07.012, 2016.

Butz, C., Grosjean, M., Goslar, T. and Tylmann, W.: Hyperspectral imaging of sedimentary bacterial pigments: a

1700-year history of meromixis from varved Lake Jaczno, northeast Poland, J. Paleolimnol., 58(1), 57–72, doi:10.1007/s10933-017-9955-1, 2017.

Cartaxana, P., Jesus, B. and Brotas, V.: Pheophorbide and pheophytin a-like pigments as useful markers for intertidal microphytobenthos grazing by Hydrobia ulvae, Estuar. Coast. Shelf Sci., 58(2), 293–297, doi:https://doi.org/10.1016/S0272-7714(03)00081-7, 2003.

Costa, K. M., Russell, J. M., Vogel, H. and Bijaksana, S.: Hydrological connectivity and mixing of Lake Towuti, Indonesia in response to paleoclimatic changes over the last 60,000years, Palaeogeogr. Palaeoclimatol. Palaeoecol., 417, 467–475, doi:https://doi.org/10.1016/j.palaeo.2014.10.009, 2015.

Croudace, I. W. and Rothwell, R. G.: Future Developments and Innovations in High-Resolution Core Scanning, in Micro-XRF Studies of Sediment Cores. Developments in Paleoenvironmental Research, edited by I. Croudace and R. Rothwell, pp. 627–647, Springer, Dordrecht., 2015.

Czernecki, B. and Miętus, M.: The thermal seasons variability in Poland, 1951–2010, Theor. Appl. Climatol., 127(1), 481–493, doi:10.1007/s00704-015-1647-z, 2017.

Diaz, R. and Rosenberg, R.: Spreading Dead Zones and Consequences for Marine Ecosystems, Science, 321, 926–929, doi:10.1126/science.1156401, 2008.

Engel, M. and Sobczak, C.: Nie tylko archeologia. Interdyscyplinarne badania wielokulturowego zespołu osadniczego w Szurpiłach na Suwalszczyźnie., Pruthenia, 7, 137–157 [online] Available from: https://d1wqtxts1xzle7.cloudfront.net/33693318/Pruthenia_7_2012_Engel-C_Sobczak-C_Nie_tylko_archeologia_Interdyscyplinarne_badania_w_Szurpilach.pdf?1400025472=&response-content-disposition=inline%3B+filename%3DNie_tylko_archeologia_Interdyscyplinarne.pdf&, 2012.

Enters, D., Kirilova, E., Lotter, A. F., Lücke, A., Parplies, J., Jahns, S., Kuhn, G. and Zolitschka, B.: Climate change and human impact at Sacrower See (NE Germany) during the past 13,000 years: A geochemical record, J. Paleolimnol., 43(4), 719–737, doi:10.1007/s10933-009-9362-3, 2010.

Fiedor, J., Fiedor, L., Kammhuber, N., Scherz, A. and Scheer, H.: Photodynamics of the bacterlochlorophyll-carotenoid system. 2. Influence of central metal, solvent and beta-carotene on photobleaching of bacteriochlorophyll derivatives, Photochem. Photobiol., 76(2), 145–152, doi:https://doi.org/10.1562/0031-8655(2002)076<0145:potbcs>2.0.co;2, 2002.

Friedrich, J., Janssen, F., Aleynik, D., Bange, H. W., Boltacheva, N., Çagatay, M. N., Dale, A. W., Etiope, G., Erdem, Z., Geraga, M., Gilli, A., Gomoiu, M. T., Hall, P. O. J. J., Hansson, D., He, Y., Holtappels, M., Kirf, M. K., Kononets, M., Konovalov, S., Lichtschlag, A., Livingstone, D. M., Marinaro, G., Mazlumyan, S., Naeher, S., North, R. P., Papatheodorou, G., Pfannkuche, O., Prien, R., Rehder, G., Schubert, C. J., Soltwedel, T., Sommer, S., Stahl, H., Stanev, E. V., Teaca, A., Tengberg, A., Waldmann, C., Wehrli, B. and Wenzhöfer, F.: Investigating hypoxia in aquatic environments: Diverse approaches to addressing a complex phenomenon, Biogeosciences, 11(4), 1215–1259, doi:10.5194/bg-11-1215-2014, 2014.

Gächter, R.: Lake restoration. Why oxygenation and artificial mixing cannot substitute for a decrease in the external phosphorus loading, Swiss J. Hydrol., 49(2), 170–185, doi:10.1007/BF02538501, 1987.

Gałka, M.: Pattern of plant succession from eutrophic lake to ombrotrophic bog in NE Poland over the last 9400 years based on high-resolution macrofossil analysis, Ann. Bot. Fenn., 51(1), 1–21, doi:10.5735/085.051.0101, 2014.

Gassner, S., Gobet, E., Schwörer, C., van Leeuwen, J., Vogel, H., Giagkoulis, T., Makri, S., Grosjean, M., Panajiotidis, S., Hafner, A. and Tinner, W.: 20,000 years of interactions between climate, vegetation and land

585 use in Northern Greece, Veg. Hist. Archaeobot., 29(1), 75–90, doi:10.1007/s00334-019-00734-5, 2020.

586 Guilizzoni, P. and Lami, A.: Paleolimnology: Use of Algal Pigments as Indicators, in Encyclopedia of

587 Environmental Microbiology, edited by G. Bitton, pp. 2306–2317, John Wiley & Sons, Inc., 2002.

588 Guilizzoni, P., Bonomi, G., Galanti, G. and Ruggiu, D.: Paleolimnology: Relationship between sedimentary

589 pigments and primary production: evidence from core analyses of twelve Italian lakes, in Hydrobiologia, vol.

590 103, edited by J. Meriläinen, P. Huttunen, and R. W. Battarbee, pp. 103–106, Kluwer Academic Publishers, The

591 Hague, Netherlands., 1983.

592 Guilizzoni, P., Lami, A., Marchetto, A., Jones, V., Manca, M. and Bettinetti, R.: Palaeoproductivity and

593 environmental changes during the Holocene in central Italy as recorded in two crater lakes (Albano and Nemi),

594 Quat. Int., 88(1), 57–68, doi:10.1016/S1040-6182(01)00073-8, 2002.

595 Heikkilä, M. and Seppä, H.: Holocene climate dynamics in Latvia, eastern Baltic region: A pollen-based summer

596 temperature reconstruction and regional comparison, Boreas, 39(4), 705–719, doi:10.1111/j.1502-

597 3885.2010.00164.x, 2010.

598 Heiri, O., Lotter, A. F. and Lemcke, G.: Loss on ignition as a method for estimating organic and carbonate

599 content in sediments: reproducibility and comparability of results, J. Paleolimnol., 25(1), 101–110, 2001.

600 Howarth, R. W., Chan, F. and Marino, R.: Do top-down and bottom-up controls interact to exclude nitrogen-

601 fixing cyanobacteria from the plankton of estuaries? An exploration with a simulation model, Biogeochemistry,

602 46(1–3), 203–231, doi:10.1007/BF01007580, 1999.

603 Hubas, C., Jesus, B., Passarelli, C. and Jeanthon, C.: Tools providing new insight into coastal anoxygenic purple

604 bacterial mats: Review and perspectives, Res. Microbiol., 162(9), 858–868, doi:10.1016/j.resmic.2011.03.010,

605 2011.

606 Hubas, C., Jesus, B., Ruivo, M., Meziane, T., Thiney, N., Davoult, D., Spilmont, N., Paterson, D. M. and

607 Jeanthon, C.: Proliferation of purple sulphur bacteria at the sediment surface affects intertidal mat diversity and

608 functionality, PLoS One, 8(12), 1–13, doi:10.1371/journal.pone.0082329, 2013.

609 Hurley, J. P.: Analysis of aquatic pigments by high performance liquid chromatography, J. Anal. Purif., 3, 12–

610 16, 1988.

611 IMGW-PIB: Suwałki Meteorological Station, Inst. Meteorol. Water Manag. [online] Available from:

612 https://danepubliczne.imgw.pl/#wprowadzenie, 2017.

613 Imhoff, J. F.: Biology of Green Sulfur Bacteria, eLS, doi:doi:10.1002/9780470015902.a0000458.pub2, 2014.

614 Itoh, N., Tani, Y., Nagatani, T. and Soma, M.: Phototrophic activity and redox condition in Lake Hamana, Japan,

615 indicated by sedimentary photosynthetic pigments and molybdenum over the last ~250 years, J. Paleolimnol.,

616 29(4), 403–422, doi:10.1023/A:1024407210928, 2003.

617 Jeffrey, S., Wright, S. and Zapata, M.: Phytoplankton Pigments., 2011.

618 Jeffrey, S. W. and Humphrey, G. F.: New spectrophotometric equations for determining chlorophylls a, b, c1 and

619 c2 in higher plants, algae and natural phytoplankton, Biochem. und Physiol. der Pflanz., 167(2), 191–194,

620 doi:10.1016/S0015-3796(17)30778-3, 1975.

621 Jenny, J.-P., Francus, P., Normandeau, A., Lapointe, F., Perga, M. E., Ojala, A., Schimmelmann, A. and

622 Zolitschka, B.: Global spread of hypoxia in freshwater ecosystems during the last three centuries is caused by

623 rising local human pressure, Glob. Chang. Biol., 22(4), 1481–1489, doi:https://doi.org/10.1111/gcb.13193,

624 2016a.

625 Jenny, J.-P., Normandeau, A., Francus, P., Taranu, Z. E., Gregory-Eaves, I., Lapointe, F., Jautzy, J., Ojala, A. E.

K., Dorioz, J.-M., Schimmelmann, A. and Zolitschka, B.: Urban point sources of nutrients were the leading cause for the historical spread of hypoxia across European lakes, Proc. Natl. Acad. Sci., 113(45), 12655–12660, doi:https://doi.org/10.1073/pnas.1605480113, 2016b.

Kinder, M., Tylmann, W., Bubak, I., Fiłoc, M., Gąsiorowski, M., Kupryjanowicz, M., Mayr, C., Sauer, L., Voellering, U. and Zolitschka, B.: Holocene history of human impacts inferred from annually laminated sediments in Lake Szurpiły, northeast Poland, J. Paleolimnol., 61(4), 419–435, doi:10.1007/s10933-019-00068-2, 2019.

Kinder, M., Tylmann, W., Rzeszewski, M. and Zolitschka, B.: Varves and mass-movement deposits record distinctly different sedimentation dynamics since the late glacial (Lake Szurpiły, northeastern Poland), Quat. Res. (United States), 93(1), 299–313, doi:10.1017/qua.2019.61, 2020.

Koinig, K. A., Shotyk, W., Lotter, A. F., Ohlendorf, C. and Sturm, M.: 9000 years of geochemical evolution of lithogenic major and trace elements in the sediment of an alpine lake - the role of climate, vegetation, and land-use history, J. Paleolimnol., 30(3), 307–320, 2003.

Kosourov, S., Murukesan, G., Jokela, J. and Allahverdiyeva, Y.: Carotenoid biosynthesis in calothrix sp. 336/3: Composition of carotenoids on full medium, during diazotrophic growth and after long-term H2 photoproduction, Plant Cell Physiol., 57(11), 2269–2282, doi:10.1093/pcp/pcw143, 2016.

Krzywicki, T.: The maximum ice sheet limit of the Vistulian Glaciation in northeastern Poland and neighbouring areas, Geol. Q., 46(2), 165–188, 2002.

Lami, A., Niessen, F., Guilizzoni, P., Masaferro, J. and Belis, C. A.: Palaeolimnological studies of the eutrophication of volcanic Lake Albano (Central Italy), J. Paleolimnol., 10(3), 181–197, 1994.

Lami, A., Guilizzoni, P. and Marchetto, A.: High resolution analysis of fossil pigments, carbon, nitrogen and sulphur in the sediment of eight European Alpine lakes: the MOLAR project, edited by A. Lami, N. Cameron, and A. Korhola, J. Limnol., 59(1), 15–28, 2000.

Leavitt, P. R.: A review of factors that regulate carotenoid and chlorophyll deposition and fossil pigment abundance, J. Paleolimnol., 9, 109–127, 1993.

Leavitt, P. R. and Hodgson, D.: Sedimentary Pigments, in Tracking Environmental Change Using Lake Sediments, vol. 3, edited by J. Smol, H. Birks, and W. Last, pp. 295–325, Kluwer, Dordrecht., 2001.

Legendre, P. and Legendre, L.: Numerical ecology. 2nd, Amsterdam., 1998.

Little, J. L., Quinlan, R., Smol, J. P. and Hall, R. I.: Past trophic status and hypolimnetic anoxia during eutrophication and remediation of Gravenhurst Bay, Ontario: Comparison of diatoms, chironomids, and historical records, Can. J. Fish. Aquat. Sci., 57(2), 333–341, doi:10.1139/f99-235, 2000.

Lotter, A. F.: Late-glacial and Holocene vegetation history and dynamics as shown by pollen and plant macrofossil analyses in annually laminated sediments from Soppensee, central Switzerland, Veg. Hist. Archaeobot., 8(3), 165–184, doi:10.1007/BF02342718, 1999.

Lürling, M., Mello, M. M., van Oosterhout, F., Domis, L. de S. and Marinho, M. M.: Response of natural cyanobacteria and algae assemblages to a nutrient pulse and elevated temperature, Front. Microbiol., 9(AUG), doi:10.3389/fmicb.2018.01851, 2018.

Madigan, M. T. and Jung, D. O.: An Overview of Purple Bacteria: Systematics, Physiology, and Habitats, in The Purple Phototrophic Bacteria. Advances in Photosynthesis and Respiration, edited by C. N. Hunter, F. Daldal, M. C. Thurnauer, and J. T. Beatty, pp. 1–15, Springer, Dordrecht., 2009.

Makri, S., Lami, A., Lods-Crozet, B. and Loizeau, J.-L.: Reconstruction of trophic state shifts over the past

667    90 years in a eutrophicated lake in western Switzerland, inferred from the sedimentary record of photosynthetic

668    pigments, J. Paleolimnol., 61(2), doi:10.1007/s10933-018-0049-5, 2019.

669    Makri, S., Rey, F., Gobet, E., Gilli, A., Tinner, W. and Grosjean, M.: Early human impact in a 15,000-year high-

670    resolution hyperspectral imaging record of paleoproduction and anoxia from a varved lake in Switzerland, Quat.

671    Sci. Rev., 239, 106335, doi:https://doi.org/10. 1016/j.quascirev.2020.106335, 2020.

672    Manske, A. K., Glaeser, J., Kuypers, M. M. M. and Overmann, J.: Physiology and Phylogeny of Green Sulfur

673    Bacteria Forming a Monospecific Phototrophic Assemblage at a Depth of 100 Meters in the Black Sea, Appl.

674    Environ. Microbiol., 71(12), 8049 LP – 8060, doi:10.1128/AEM.71.12.8049-8060.2005, 2005.

675    Mantoura, R. F. C. and Llewellyn, C. A.: The rapid determination of algal chlorophyll and carotenoid pigments

676    and their breakdown products in natural waters by reverse-phase high-performance liquid chromatography, Anal.

677    Chim. Acta, 151(Supplement C), 297–314, 1983.

678    Marcisz, K., Kołaczek, P., Gałka, M., Diaconu, A.-C. and Lamentowicz, M.: Exceptional hydrological stability

679    of a Sphagnum-dominated peatland over the late Holocene, Quat. Sci. Rev., 231, 106180,

680    doi:https://doi.org/10.1016/j.quascirev.2020.106180, 2020.

681    Meyers, P. A.: Applications of organic geochemistry to paleolimnological reconstructions: A summary of

682    examples from the Laurentian Great Lakes, in Organic Geochemistry, vol. 34, pp. 261–289, Pergamon., 2003.

683    Montesinos, E., Guerrero, R., Abella, C. and Esteve, I.: Ecology and Physiology of the Competition for Light

684    Between Chlorobium limicola and Chlorobium phaeobacteroides in Natural Habitats, Appl. Environ. Microbiol.,

685    46(5), 1007–1016, doi:10.1128/aem.46.5.1007-1016.1983, 1983.

686    Munsell Color (Firm): Munsell soil color charts : with genuine Munsell color chips, 2009 year revised. Grand

687    Rapids, MI : Munsell Color, 2010. [online] Available from:

688    https://search.library.wisc.edu/catalog/9910109259802121, 2010.

689    Murtagh, F. and Legendre, P.: Ward's Hierarchical Agglomerative Clustering Method: Which Algorithms

690    Implement Ward's Criterion?, J. Classif., 31(3), 274–295, doi:10.1007/s00357-014-9161-z, 2014.

691    Naeher, S., Smittenberg, R. H., Gilli, A., Kirilova, E. P., Lotter, A. F. and Schubert, C. J.: Impact of recent lake

692    eutrophication on microbial community changes as revealed by high resolution lipid biomarkers in Rotsee

693    (Switzerland), Org. Geochem., 49, 86–95, doi:10.1016/j.orggeochem.2012.05.014, 2012.

694    Naeher, S., Gilli, A., North, R. P., Hamann, Y. and Schubert, C. J.: Tracing bottom water oxygenation with

695    sedimentary Mn/Fe ratios in Lake Zurich, Switzerland, Chem. Geol., 352, 125–133,

696    doi:10.1016/j.chemgeo.2013.06.006, 2013.

697    Oksanen, J., Kindt, R., Pierre, L., O'Hara, B., Simpson, G. L., Solymos, P., Stevens, M. H. . H. H., Wagner, H.,

698    Blanchet, F. G., Kindt, R., Legendre, P., Minchin, P. R., O'Hara, R. B., Simpson, G. L., Solymos, P., Stevens,

699    M. H. . H. H. and Wagner, H.: vegan: Community Ecology Package, R package version 2.4-0, R Packag. version

700    2.2-1 [online] Available from: http://vegan.r-forge.r-project.org, 2016.

701    Oren, A.: 12 - Characterization of Pigments of Prokaryotes and Their Use in Taxonomy and Classification, in

702    Taxonomy of Prokaryotes, vol. 38, edited by F. Rainey and A. B. T.-M. in M. Oren, pp. 261–282, Academic

703    Press., 2011.

704    Parkin, T. B. and Brock, T. D.: Photosynthetic bacterial production in lakes: The effects of light intensity,

705    Limnol. Oceanogr., 25(4), 711–718, doi:10.4319/lo.1980.25.4.0711, 1980.

706    Pearson, F. J. and Coplen, T. B.: Stable Isotope Studies of Lakes, in Lakes, edited by A. Lerman, pp. 325–339,

707    Springer, New York, NY., 1978.

708  Poraj-Górska, A. I., Żarczyński, M. J., Ahrens, A., Enters, D., Weisbrodt, D. and Tylmann, W.: Impact of

709  historical land use changes on lacustrine sedimentation recorded in varved sediments of Lake Jaczno,

710  northeastern Poland, Catena, 153, 182–193, doi:10.1016/j.catena.2017.02.007, 2017.

711  R Core Team: R: A language and environment for statistical computing., [online] Available from: http://www.r-

712  project.org, 2015.

713  Reimer, P. J., Bard, E., Bayliss, A., Beck, J. W., Blackwell, P. G., Ramsey, C. B., Buck, C. E., Cheng, H.,

714  Edwards, R. L., Friedrich, M., Grootes, P. M., Guilderson, T. P., Haflidason, H., Hajdas, I., Hatté, C., Heaton, T.

715  J., Hoffmann, D. L., Hogg, A. G., Hughen, K. A., Kaiser, K. F., Kromer, B., Manning, S. W., Niu, M., Reimer,

716  R. W., Richards, D. A., Scott, E. M., Southon, J. R., Staff, R. A., Turney, C. S. M. and van der Plicht, J.:

717  IntCal13 and Marine13 Radiocarbon Age Calibration Curves 0–50,000 Years cal BP, Radiocarbon, 55(4), 1869–

718  1887, doi:10.2458/azu_js_rc.55.16947, 2013.

719  Sanchini, A., Szidat, S., Tylmann, W., Vogel, H., Wacnik, A. and Grosjean, M.: A Holocene high-resolution

720  record of aquatic productivity, seasonal anoxia and meromixis from varved sediments of Lake Łazduny, North-

721  Eastern Poland: insight from a novel multi-proxy approach, J. Quat. Sci., in press, 2020.

722  Schindler, D. W.: Recent advances in the understanding and management of eutrophication, Limnol. Oceanogr.,

723  51(1part2), 356–363, doi:https://doi.org/10.4319/lo.2006.51.1_part_2.0356, 2006.

724  Schneider, T., Rimer, D., Butz, C. and Grosjean, M.: A high-resolution pigment and productivity record from the

725  varved Ponte Tresa basin (Lake Lugano, Switzerland) since 1919: insight from an approach that combines

726  hyperspectral imaging and high-performance liquid chromatography, J. Paleolimnol., 60(3), 381–398,

727  doi:10.1007/s10933-018-0028-x, 2018.

728  Schnurrenberger, D., Russell, J. and Kelts, K.: Classification of lacustrine sediments based on sedimentary

729  components, J. Paleolimnol., 29(2), 141–154, doi:10.1023/A:1023270324800, 2003.

730  Smith, V. H. and Schindler, D. W.: Eutrophication science: where do we go from here?, Trends Ecol. Evol.,

731  24(4), 201–207, doi:https://doi.org/10.1016/j.tree.2008.11.009, 2009.

732  Smol, J. P.: The power of the past: using sediments to track the effects of multiple stressors on lake ecosystems,

733  Freshw. Biol., 55(Suppl. 1), 43–59, doi:doi:10.1111/j.1365-2427.2009.02373.x, 2010.

734  Stuiver, M. and Reimer, P. J.: Extended 14C data base and revised CALIB 3.0 14C age calibration program,

735  Radiocarbon, 35(1), 215–230, doi:10.1017/S0033822200013904, 1993.

736  Szidat, S., Salazar, G. A., Vogel, E., Battaglia, M., Wacker, L., Synal, H.-A. and Türler, A.: 14C Analysis and

737  Sample Preparation at the New Bern Laboratory for the Analysis of Radiocarbon with AMS (LARA),

738  Radiocarbon, 56(02), 561–566, doi:10.1017/s0033822200049602, 2014.

739  Tõnno, I., Nauts, K., Belle, S., Nõmm, M., Freiberg, R., Kõiv, T. and Alliksaar, T.: Holocene shifts in the

740  primary producer community of large, shallow European Lake Peipsi, inferred from sediment pigment analysis,

741  J. Paleolimnol., 61(4), 403–417, doi:10.1007/s10933-019-00067-3, 2019.

742  Tu, L., Jarosch, K. A., Schneider, T. and Grosjean, M.: Phosphorus fractions in sediments and their relevance for

743  historical lake eutrophication in the Ponte Tresa basin (Lake Lugano, Switzerland) since 1959, Sci. Total

744  Environ., 685, 806–817, doi:10.1016/j.scitotenv.2019.06.243, 2019.

745  Tylmann, W., Zolitschka, B., Enters, D. and Ohlendorf, C.: Laminated lake sediments in northeast Poland:

746  Distribution, preconditions for formation and potential for paleoenvironmental investigation, J. Paleolimnol.,

747  50(4), 487–503, doi:10.1007/s10933-013-9741-7, 2013.

748  Vitousek, P. M., Cassman, K., Cleveland, C., Crews, T., Field, C. B., Grimm, N. B., Howarth, R. W., Marino,

R., Martinelli, L., Rastetter, E. B. and Sprent, J. I.: Towards an ecological understanding of biological nitrogen fixation, in Biogeochemistry, vol. 57–58, pp. 1–45., 2002.

Weisbrodt, D., Enters, D., Żarczyński, M. J., Poraj-Górska, A. I. and Tylmann, W.: Contribution of non-pollen palynomorphs to reconstructions of land-use changes and lake eutrophication: case study from Lake Jaczno, northeastern Poland, Limnol. Rev., 16(4), 247–256, doi:10.1515/limre-2016-0027, 2017.

Wetzel, R. G.: Limnology: Lake and River Ecosystems, 3rd ed., Acedemic Press., 2001.

Wirth, S. B., Gilli, A., Niemann, H., Dahl, T. W., Ravasi, D., Sax, N., Hamann, Y., Peduzzi, R., Peduzzi, S., Tonolla, M., Lehmann, M. F. and Anselmetti, F. S.: Combining sedimentological, trace metal (Mn, Mo) and molecular evidence for reconstructing past water-column redox conditions: The example of meromictic Lake Cadagno (Swiss Alps), Geochim. Cosmochim. Acta, 120, 220–238, doi:10.1016/j.gca.2013.06.017, 2013.

Woolway, R. I. and Merchant, C. J.: Worldwide alteration of lake mixing regimes in response to climate change, Nat. Geosci., 12(4), 271–276, doi:10.1038/s41561-019-0322-x, 2019.

Yurkov, V. V and Beatty, J. T.: Aerobic Anoxygenic Phototrophic Bacteria, Microbiol. Mol. Biol. Rev., 62(3), 695 LP – 724 [online] Available from: http://mmbr.asm.org/content/62/3/695.abstract, 1998.

Zander, P. D., Szidat, S., Kaufman, D. S., Żarczyński, M., Poraj-górska, A. I. and Grosjean, M.: Miniature radiocarbon measurements (< 150 μg C ) from sediments of Lake Żabińskie , Poland : effect of precision and dating density on age- depth models, Geochronology, 2(April), 63–79, doi:10.5194/gchron-2-63-2020, 2020.

Zolitschka, B., Francus, P., Ojala, A. E. K. and Schimmelmann, A.: Varves in lake sediments - a review, Quat. Sci. Rev., 117, 1–41, doi:10.1016/j.quascirev.2015.03.019, 2015.

Züllig, H.: Untersuchungen über die Stratigraphie von Carotinoiden im geschichteten Sediment von 10 Schweizer Seen zur Erkundung früherer Phytoplankton-Entfaltungen, Schweizerische Zeitschrift für Hydrol., 44(1), 1–98, 1982.

Züllig, H.: Role of carotenoids in lake sediments for reconstructing trophic history during the late Quaternary, J. Paleolimnol., 2(1), 23–40, doi:10.1007/BF00156982, 1989.
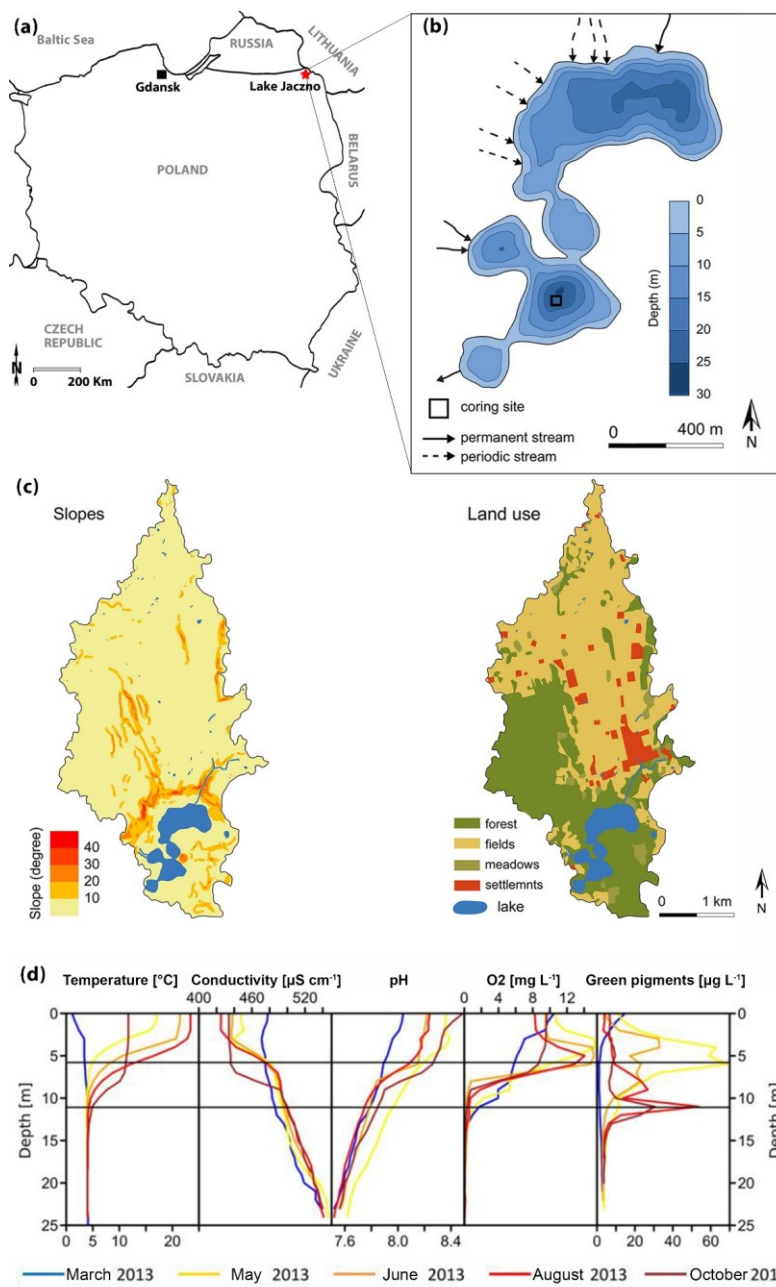
790

791
792
793
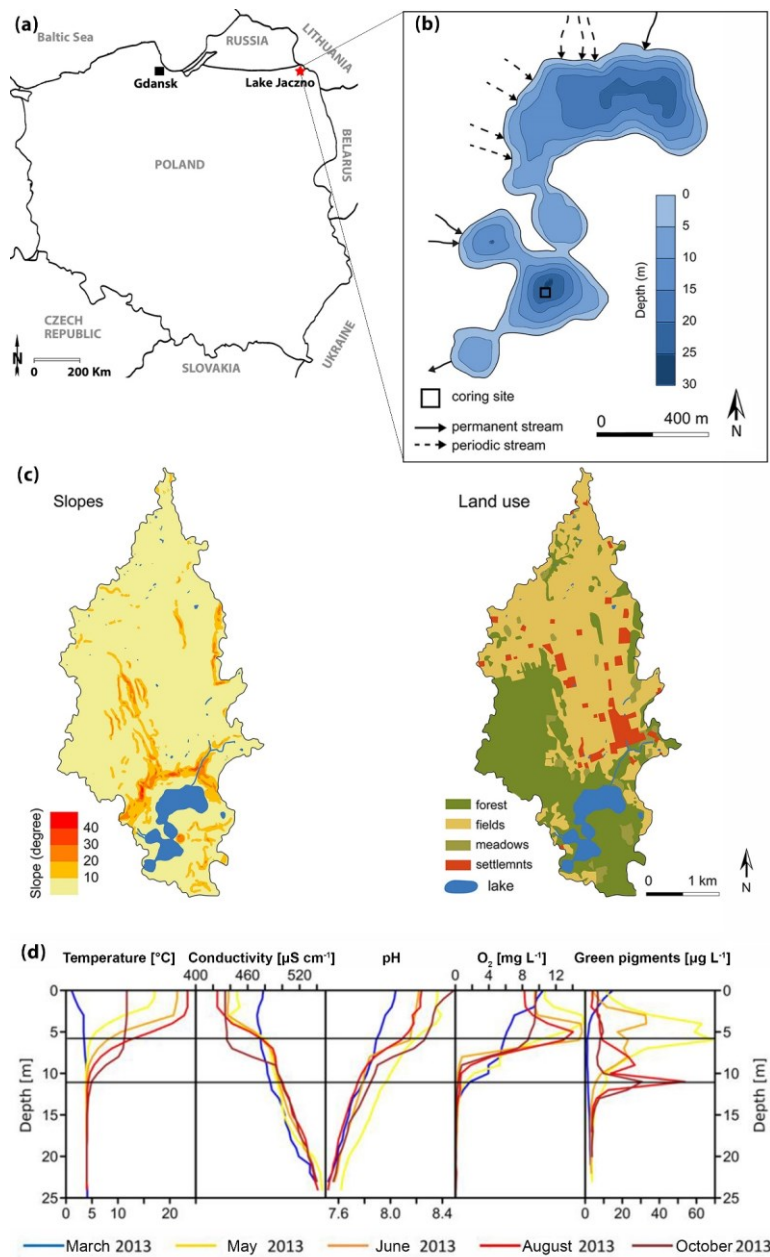
794
795  **Figure 1: a) Localization of Lake Jaczno. b) Lake bathymetry (modified from Poraj-Górska et al., 2017) and coring**
796  **position c) Slopes and land use maps of the catchment (modified from Poraj-Górska et al., 2017) d) Seasonal limnological**
797  **parameters in 2013 CE (Butz et al., 2016).**
798

799

800

801
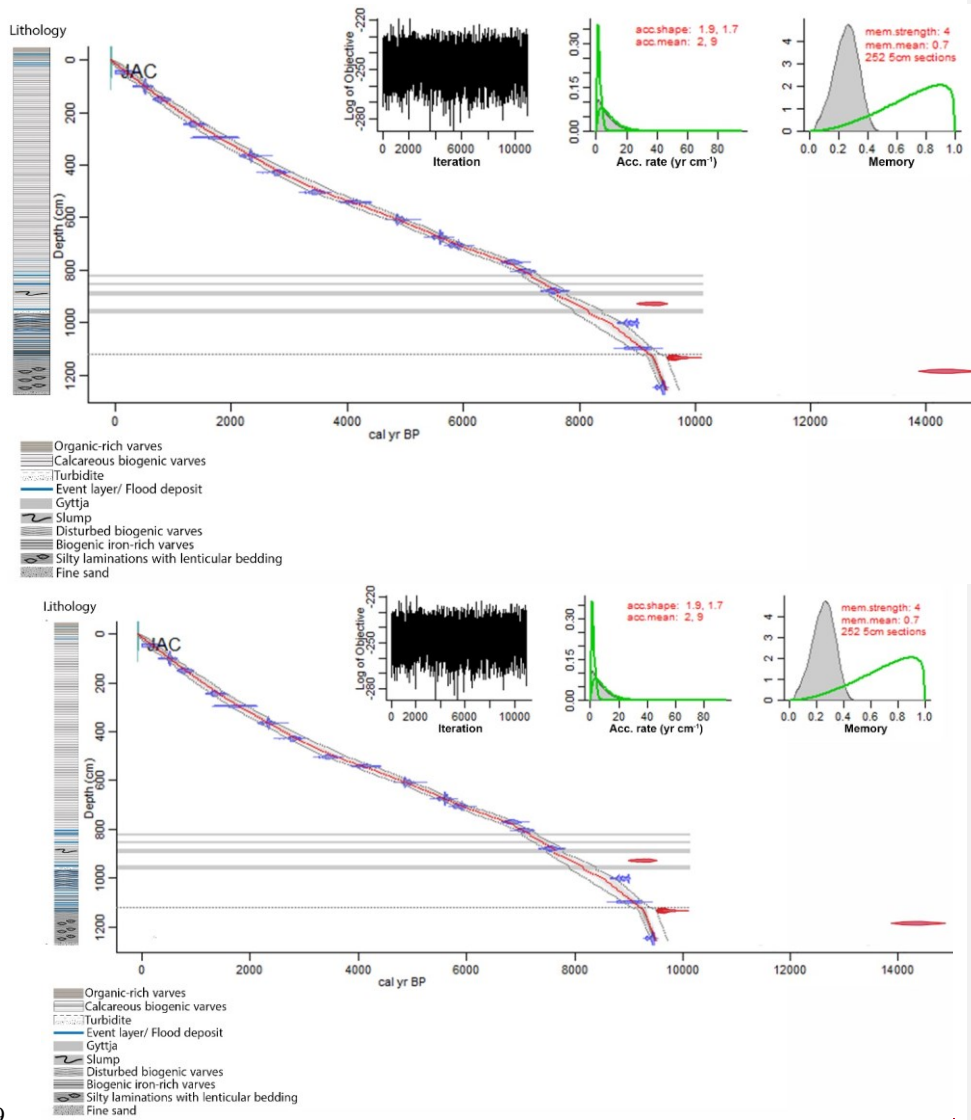
802   **Figure 2: Age depth model and lithology of Lake Jaczno. The red line is the modelled chronology using**

803   **Bacon (Blaauw and Christeny, 2011; Blaauw et al., 2020); the excluded outliers are shown in red. The**

804   **dotted lines indicate the 95 % (2σ) probabilities. The grey horizontal areas indicate event layers (>3 cm)**

805   **excluded from the model. The horizontal dashed line marks the boundary of a higher sedimentation rate**

806   **(model parameter). The upper left panel shows the log objective vs. MCMC iteration that indicates a**

807  **stationary distribution. The middle and right panels indicate the distributions (prior in green, posterior in**
808  **grey) for the accumulation rate and the memory, respectively.**

809

810

811

812

813

814

815

816

817

818

821

822
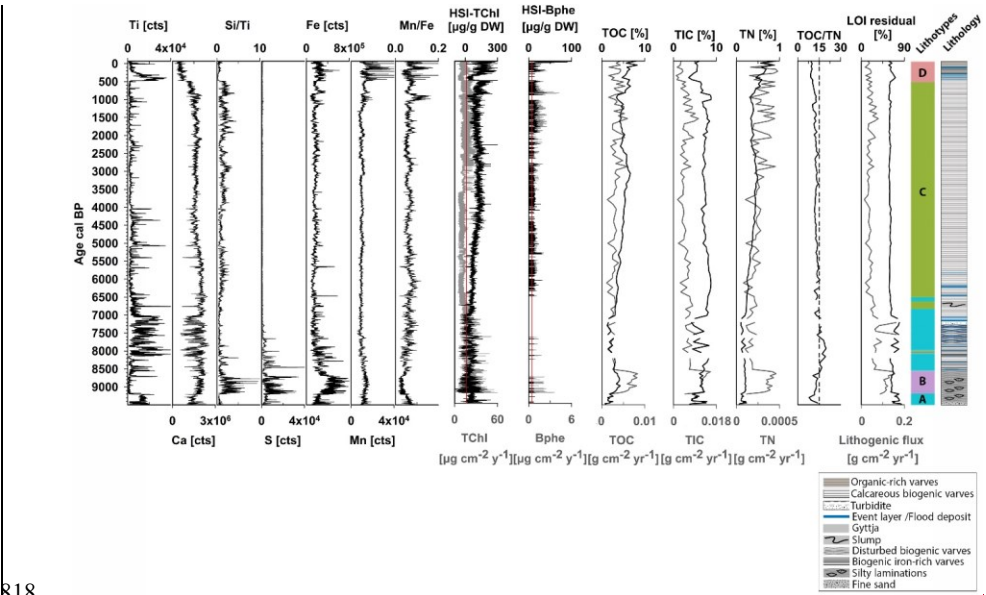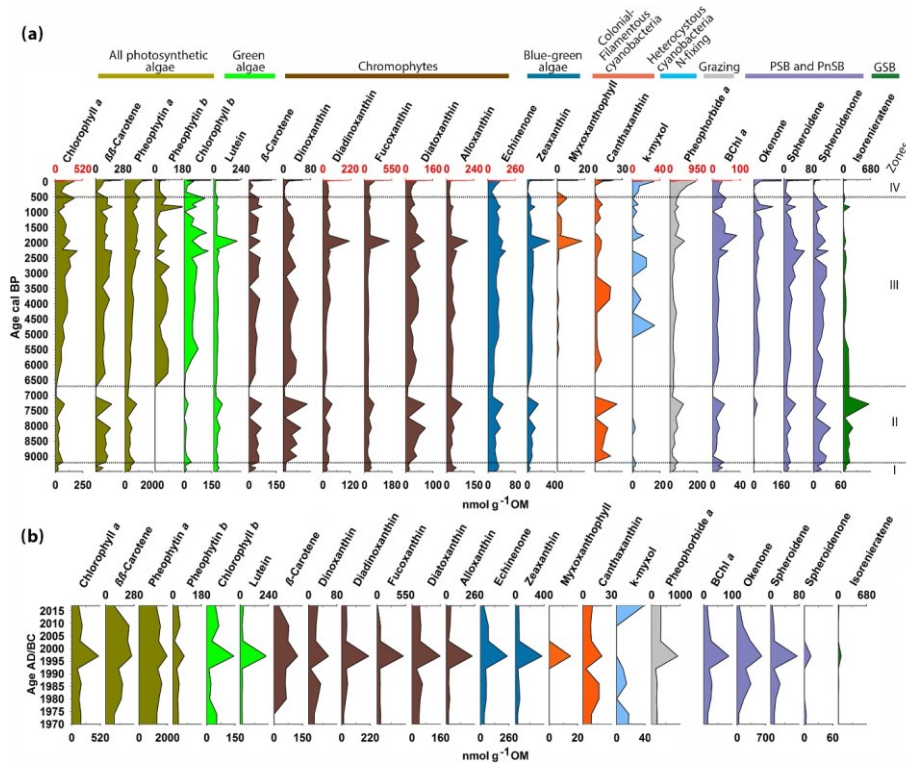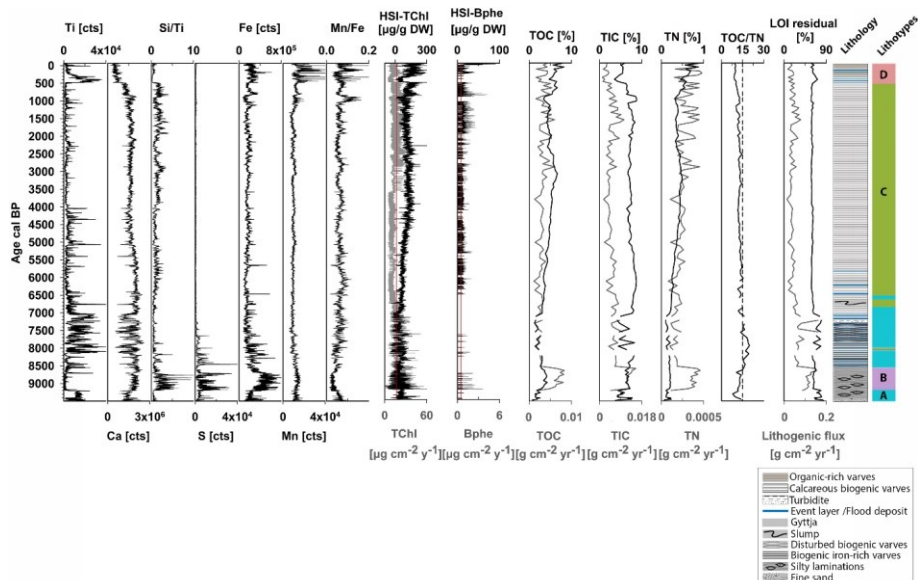
**Figure 3: Selected biogeochemical proxies that defined the four sedimentary lithotypes A–D (in different color) after unconstrained clustering and PCA analysis (Fig. S2). On the right: sediment lithology based on visual examination.**

826

827

828

829

830

831

832

833

834

835

836

837

838

839
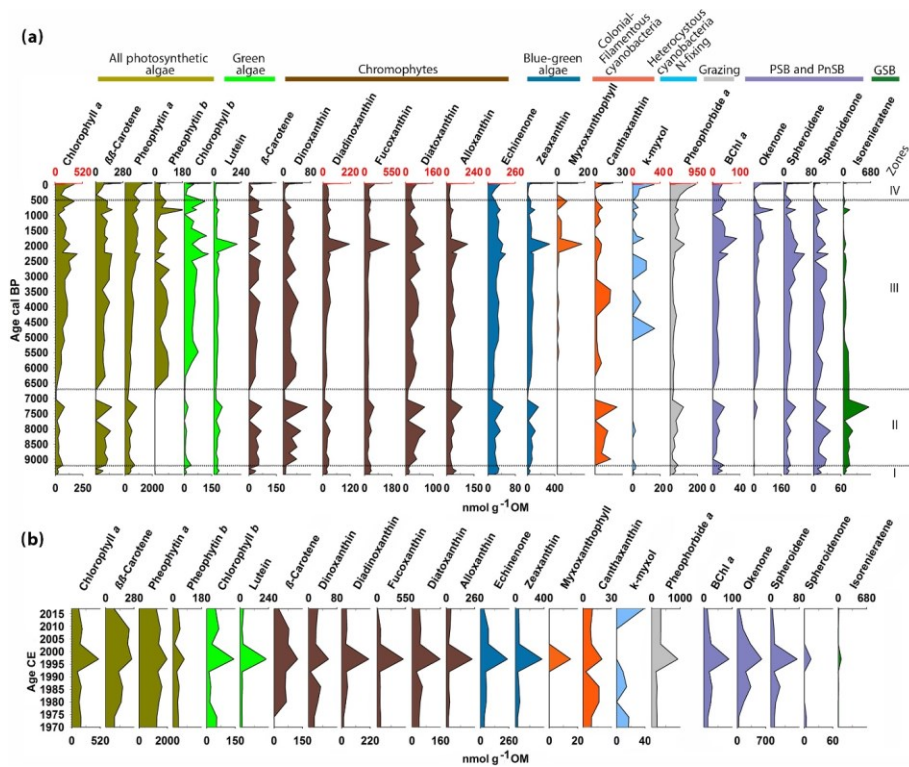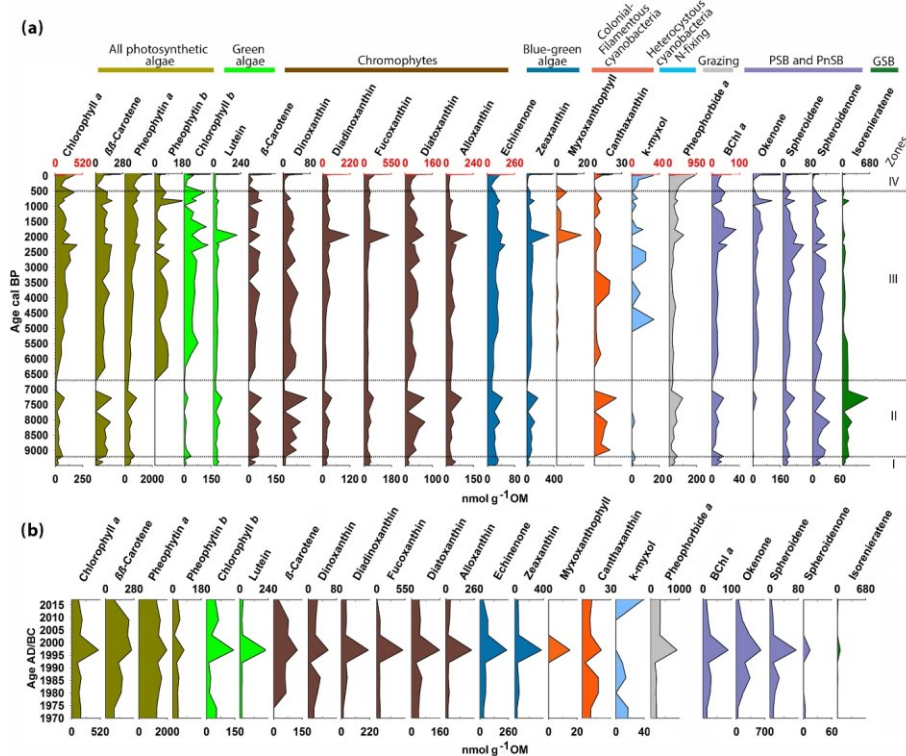
**Figure 4: Chlorophyll, chlorophyll derivatives, carotenoids and bacterial pigments concentrations measured by HPLC a) for the entire Holocene, and b) for the last 50 years. The zones are defined by constrained hierarchical clustering. The different colors indicate different algal groups based on the pigments' taxa affiliation. The occasional red scale on top marks the significantly higher concentrations of these pigments in the last 50 years.**

852
853

854
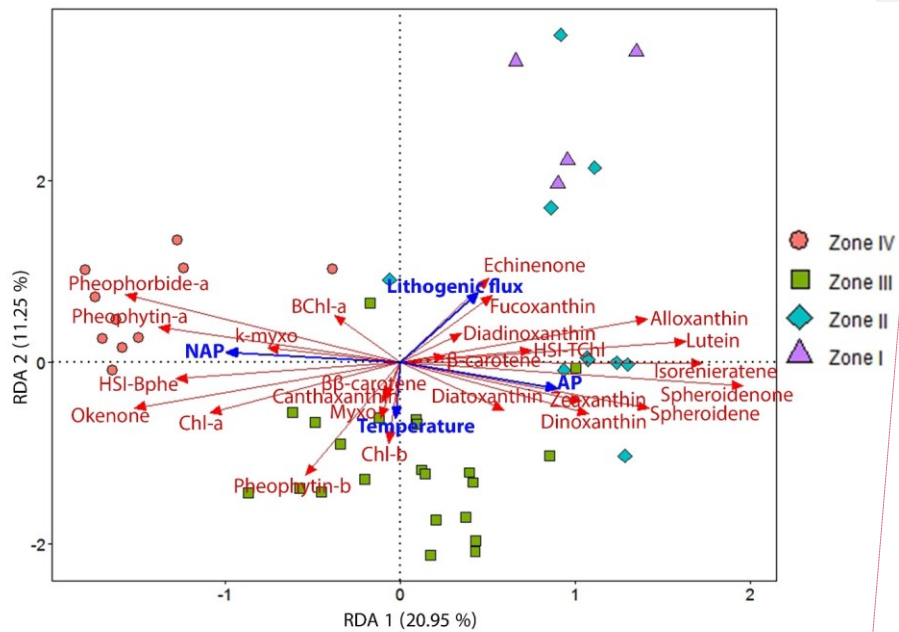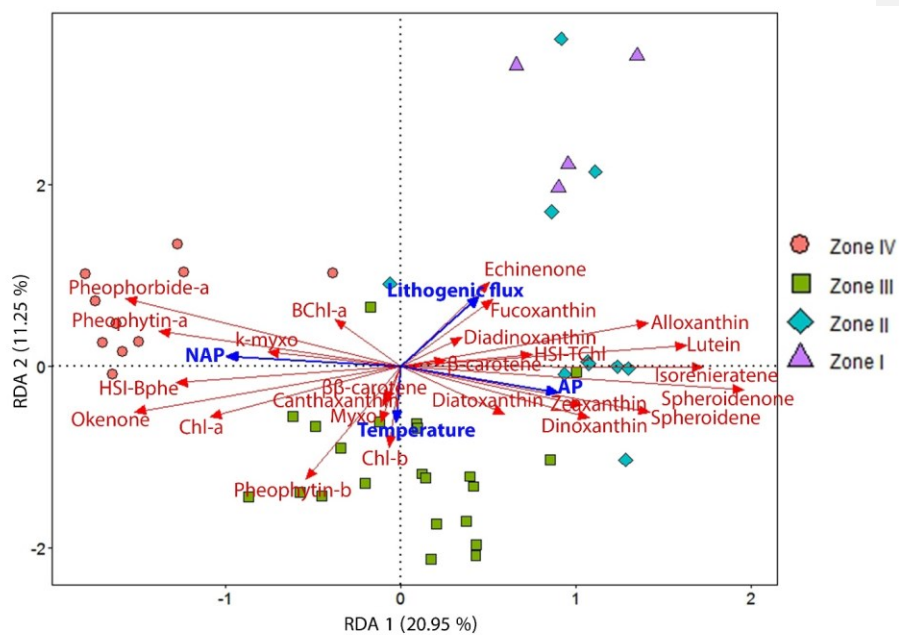
**Fig 5: RDA triplot showing the explanatory variables (AP, NAP, temperature and lithogenic flux) in blue, and the response variables (HPLC- and HSI-inferred pigment concentrations) in red. The samples are grouped according to the pigment zones (Fig. 4a).**

**Figure 6: Holocene summary of the relative abundance of purple bacteria (sum of PSB and PnSB) and GSB, *Chromatium* (okenone, PSB) and *Clorobium* (isorenieratene, GSB), the content of spheroidene and spheroidenone pigments produced by *R. sphaeroides* (PnSB), and the high-resolution calibrated HSI-TChl and HSI-Bphe concentrations. Top: indication of lithogenic flux and general evolution of the chemocline. Bottom: AP/NAP percentages (Kinder et al., 2019; Marcisz et al., 2020) with archaeological evidence of human impact, and the annual mean temperature variability (Heikkilä and Seppä, 2010).**

**Table 1: Radiocarbon age results and calibrated ages. Uncertainties for $^{14}$C ages refer to 68 % probabilities (1σ), whereas ranges of calibrated ages refer to 95 % probabilities (2σ). Outlier samples are marked with an asterisk. Indet: indeterminable, dicot: dicotyledonous.**

| Sample ID | Material | C mass (µg C) | Age $^{14}$C BP | Age (cal BP)[a] | Age range (cal BP)[b] | Graphite /Gas |
|---|---|---|---|---|---|---|
| BE-10957.1.1 | *Betula alba* fruit, woody scale, *Pinus sylvestris* needle base | 104 | 132±64 | 142 | 0–284 | gas |
| BE-10958.1.1 | *Betula alba* fruit scale, woody scale, dicot leaf fragment | 219 | 482±44 | 755 | 679–904 | graphite |
| BE-10959.1.1 | *Pinus sp.* periderm, coniferous wood and periderm fragment, *Betula alba* fruit fragments, coniferous scales | 118 | 872±55 | 790 | 694–912 | graphite |
| BE-10960.1.1 | *Pinus sp.* periderm, *Betula alba* fruit fragments, conifer scale, Pinus sp. periderm, *Betula alba* fruit fragments | 64 | 1460±67 | 1364 | 1283–1522 | gas |
| BE-10961.1.1 | *Betula alba* fruit fragments, conifer scale, *Betula alba* fruit, semi–charred periderm | 19 | 1781±127 | 1706 | 1410–1987 | gas |
| BE-10962.1.1 | *Alnus glutinosa* fruit, *Betula alba* fruit fragments, needle/leaf indet, male anthere indet | 268 | 2321±39 | 2341 | 2180–2458 | graphite |
| BE-10963.1.1 | *Betula alba* fruit fragments, *Pinus sp.* periderm, male anthere indet, *Betula alba* fruit fragments, *Pinus sp.* periderm, conifer scales | 73 | 2677±69 | 2801 | 2545–2959 | gas |
| BE-10964.1.1 | *Betula alba* fruit fragments, *Pinus sp.* periderm, male anthere indet, *Betula alba* fruit fragments | 74 | 3229±72 | 3458 | 3259–3633 | gas |
| BE-10965.1.1 | *Alnus glutinosa* fruit fragment, *Betula alba* fruit fragments, conifer scales, dicot leaf fragments | 130 | 3758±60 | 4125 | 3927–4383 | graphite |
| BE-10966.1.1 | Male anthere indet, dicot leaf fragments, conifer scales, indet scale, wood indet | 399 | 4322±36 | 4887 | 4836–4972 | graphite |
| BE-10967.1.1 | Dicot leaf fragments, indet scale, male anthere indet | 428 | 4860±37 | 5601 | 5491–5650 | graphite |

| | | | | | |
|---|---|---|---|---|---|
| *BE-10968.1.1* | Dicot leaf fragments, wood remains | 348 | 5144±39 | 5906 | 5753–5989 | graphite |
| *BE-10969.1.1* | Dicot leaf fragments, indet periderm, wood remains | 183 | 5998±57 | 6839 | 6678–6977 | graphite |
| *BE-10970.1.1* | Deciduous woody scale | 365 | 6153±41 | 7062 | 6942–7166 | graphite |
| *BE-10971.1.1* | *Betula alba* fruit fragments, *Pinus sp.* periderm, conifer scale, wood indet | 111 | 6699±79 | 7567 | 7439–7674 | graphite |
| *\*BE-10972.1.1* | *Pinus sylvestris* needle fragments, wood indet | 58 | 8291±99 | 9279 | 9029–9475 | gas |
| *BE-10973.1.1* | Dicot leaf fragments, deciduous periderm, wood indet | 996 | 8018±22 | 8896 | 8778–9007 | graphite |
| *BE-10974.1.1* | Betula alba fruit fragments, *Pinus sylvestris* needle fragments, dicot leaf fragments | 117 | 8094±91 | 9019 | 8651–9287 | gas |
| *\*BE-10975.1.1* | *Pinus sylvestris* needle fragments, *Betula alba* fruit fragments, indet periderm | 280 | 8715±54 | 9677 | 9548–9887 | graphite |
| *\*BE-10976.1.1* | Dicot. leaf fragments, male anthere indet, conifer needle tip, indet periderm | 308 | 12446±69 | 14580 | 14198–14994 | graphite |
| *BE-10977.1.1* | Dicot leaf fragments, *Pinus sp.* periderm, woody scale | 999 | 8388±22 | 9440 | 9318–9479 | graphite |

873 [a] Median probability (Stuiver and Reimer, 1993)

874 [b] Calibrated age range with the IntCal 13 calibration curve (Stuiver and Reimer, 1993; Reimer et al.,

875 2013)

876

877